A single-cell atlas of transcriptome changes in the intestinal epithelium at the suckling-to-weaning transition

Tania Malonga[1,2], Christelle Knudsen[1], Emeline Lhuillier[3], Patrick Aymard[1], Elisabeth Jones[1], Corinne Lencina[1], Manon Despeyroux[1], Elodie Riant[4], Cédric Cabau[5], Alyssa Ivy[6], Crystal L. Loving[6], Nathalie Vialaneix[2,7*], Martin Beaumont[1*#]

1 - GenPhySE, Université de Toulouse, INRAE, ENVT, 31326, Castanet Tolosan, France.

2 - Université de Toulouse, INRAE, UR MIAT, 31326, Castanet-Tolosan, France.

3 - GeT-Sante, I2MC, INSERM-Université Paul Sabatier, Plateforme Génome et Transcriptome, GenoToul, Toulouse, France.

4 - Plateau de cytométrie I2MC, INSERM, TRI-GenoToul, Université Paul Sabatier, Toulouse, France.

5 - Sigenae, GenPhySE, Université de Toulouse, INRAE, ENVT, F-31326, Castanet-Tolosan, France.

6 - Food Safety and Enteric Pathogens Research Unit, National Animal Disease Center, Agricultural Research Service, USDA, Ames, Iowa, USA.

7 - Université de Toulouse, INRAE, BioinfOmics, GenoToul Bioinformatics Facility, Castanet-Tolosan, France.

*: Contributed equally.

#: Correspondence

Email: martin.beaumont@inrae.fr

Address: 24 Chemin de Borde Rouge, 31320 Castanet Tolosan, France.

Phone: +33 5 61 28 51 85

Abstract

The suckling-to-weaning dietary transition is a key step in mammalian intestinal development. However, the relative contributions of genetically wired and nutritional factors in this maturation process remain to be elucidated. Moreover, the cellular diversity of the intestinal epithelium has been overlooked in this context. The aim of our study was to identify the transcriptome changes induced in each cell type of the intestinal epithelium at the onset of solid food ingestion. We compared the single-cell transcriptome of epithelial cells isolated from the caecum of age-matched littermate suckling rabbits ingesting or not solid food. Our dataset provides the first single-cell atlas of the rabbit intestinal epithelium and highlights the interest of the rabbit as a model for studying BEST4^{+} epithelial cells, which are absent in mice. Solid food ingestion induced extensive transcriptome changes in each epithelial cell type, with the most pronounced changes noted in absorptive and BEST4^{+} cells. Some of the effects of solid food introduction were common to most epithelial cell types, such as the upregulation of *ALDH1A1*, which encodes for a vitamin A processing enzyme. Solid food ingestion remodeled epithelial defenses systems, as observed by the increased expression of interferon-stimulated genes in mature absorptive and BEST4^{+} cells. Solid food also upregulated the gene expression of the immunoglobulin transporter *PIGR*, specifically in cells located at the base of epithelial crypts and in goblet cells. In addition, solid food triggered epithelial differentiation, which was associated with modification of the expression of genes involved in handling of amino acids, lipids and bile acids, as well as changes in hormone expression by enteroendocrine cells. These cell type-specific transcriptome modifications induced by solid food ingestion coincided with changes in microbiota composition and metabolic activity, which may contribute to epithelial maturation. Overall, our work provides a single-cell atlas of the transcriptome changes induced in the intestinal epithelium at the suckling-to-weaning transition.

Key words: weaning, epithelium, gut, postnatal development, early life, scRNA-seq

Introduction

The intestinal epithelium contributes to digestion and allows nutrient absorption while providing a physical and immunological barrier against microorganisms and toxic compounds (Peterson and Artis 2014). This dual functionality is enabled by specialized absorptive and secretory epithelial cells, all derived from actively dividing stem cells located at the crypt base (Barker 2014). Single-cell transcriptomics has recently deepened our understanding of the cellular diversity of the intestinal epithelium (Elmentaite et al. 2020; Fawkner-Corbett et al. 2021; Burclaff et al. 2022). Absorptive cells now emerge as a heterogeneous population with distinct functions along the crypt-villus axis (Moor et al. 2018; Beumer et al. 2022). Additionally, BEST4^{+} cells were recently identified as a novel subset of mature absorptive cells with potential roles in ion transport, mucus hydration, and secretion of antimicrobial peptides and hormones (Malonga et al. 2024). Broad cellular diversity is also osberved in the secretory cell lineage, as exemplified by the numerous subtypes of enteroendocrine cells defined by their hormone secretion profiles (Beumer et al. 2020). Heterogeneous populations of mucus-secreting goblet cells have also been identified along the crypt-villus axis with a zonation of their antimicrobial activities (Parikh et al. 2019; Beumer et al. 2022). However, this newly uncovered diversity of epithelial cells is minimally understood in the context of postnatal intestinal development.

After birth, the intestinal epithelium of the newborn undergoes a maturation process that culminates at the suckling-to-weaning transition (Muncan et al. 2011; Frazer and Good 2022). Indeed, the dietary switch from maternal milk to solid food is associated with an adaptation of epithelial digestion, absorption and transport systems enabling the transition from a high-fat diet to a carbohydrate-based diet (Henning 1981; Hansson et al. 2011). The onset of solid food ingestion also coincides with a reduced epithelial permeability linked to a remodeling of epithelial defense systems including tight junctions, microbial detection systems, glycosylation and secretion of antimicrobial peptides and mucus (Biol-N'garagba and Louisot 2003; Holmes et al. 2006; Ménard et al. 2008; Price et al. 2018; Navis et al. 2019). This epithelial developmental process follows a genetically wired program tuned by several factors including changes in

glucocorticoid levels, the introduction of solid food, and the cessation of suckling (Nanthakumar and Henning 1993; Muncan et al. 2011; Beaumont et al. 2022; Díez-Sánchez et al. 2024). In addition, ingestion of solid food also strongly alters the composition of the gut microbiota, which contributes to the induction of epithelial maturation, notably through the release of bacterial metabolites such as butyrate (Pan et al. 2018; Beaumont et al. 2020). A defect in host-microbiota co-maturation around weaning is known to increase the susceptibility to inflammatory or metabolic diseases later in life (Al Nabhani et al. 2019; Hornef and Torow 2020). It is therefore essential to understand the mechanisms underlying epithelial maturation at the suckling-to-weaning transition. However, a large knowledge gap exists regarding epithelial cell type-specific adaptations triggered by the introduction of solid food in the diet.

Transcriptomic regulations induced in the intestinal epithelium during the transition from milk to solid food were described in mice (Rakoff-Nahoum et al. 2015; Pan et al. 2018). However, these studies did not delineate the relative contributions of age and nutrition in epithelial maturation. In fact, controlling dietary intake in early life is difficult in mice because the stress of separation from the mother disrupts the gut barrier function (Ilchmann-Diounou and Menard 2020). In contrast, in rabbits, suckling occurs only once per day for about 5 minutes and there is naturally little contact between the mother and her litter (Gidenne and Lebas 2006). This unique behavior allows to control of milk and solid food ingestion in early life by housing separately the mother and her litter (Beaumont et al. 2022). In addition, we have recently shown that BEST4^{+} cells are present in the intestinal epithelium of rabbits, whereas these cells are absent in mice (Malonga et al. 2024). Thus, the rabbit is a valuable model to study epithelial maturation at the suckling-to-weaning transition. In this study, we used single-cell transcriptomics to identify the maturation program induced by solid food ingestion in each cell type of the intestinal epithelium of age-matched suckling rabbit littermates fed or not with solid food. In addition, analysis of the microbiota and metabolome allowed us to link the changes in luminal environment induced by solid food ingestion with the gene expression regulation observed at the single-cell level in the epithelium.

Material and methods

Animal experiments

The experiments were performed at the PECTOUL experimental facility (GenPhySE, INRAE, Toulouse, France). The handling of rabbits followed the recommendations outlined by the European Union's regulations for the protection of animals used in scientific research (2010/63/EU), and was consistent with the French legislation (NOR: AGRG1238753A 2013). This project received approval from the local ethics committee "Comité d'éthique en expérimentation animale SCIENCE ET SANTE ANIMALES" N°115 (SSA_2022_012 and SSA_2024_004V2). Multiparous dams (n = 4) were housed individually in wire cages (61 × 68 × 50 cm) equipped with a closed nest (39 × 27 × 50 cm). The litter size was limited to 10 pups per litter (Figure S1A). From postnatal day (PND) 4, pups were placed in a new cage, adjacent to their mother's cage. At PND12, litter sizes were reduced to 6 pups in order to maximize milk ingestion. Pups from each litter were separated in 2 cages on either side of their mother's cage (3 pups/cage) to form two groups. In the first group (Milk), the pups were exclusively suckling. In the second group (Milk+Solid), the pups were suckling while having *ad libitum* access to commercial solid food pellets (StabiGreen, Terrya). During the whole experiment, the dam and the pups were placed once a day for 5-10 minutes in the nest of the dam's cage for suckling before returning to their respective cages. Coprophagia was prevented by removing feces dropped by the mother in the nest after each suckling. Individual milk intake was quantified daily (from PND12 onwards) by weighing pups before and after suckling. Solid feed intake was measured daily at the cage level (3 pups) by weighing the feeder. The experiment was repeated a second time independently with n = 5 litters in order to collect samples for RNA *in situ* hybridization, immunohistochemistry, electron microscopy and calprotectin measurements. All other measurements were performed on samples collected during the first experiment.

Sample collection

One male pup per litter (n = 4) and per group (Milk or Milk+Solid) was sacrificed after suckling at PND24 or PND25 by electronarcosis followed by exsanguination. Blood collected in EDTA tubes was

centrifuged (1000 × g, 10 min, 4°C) and plasma was stored at -20°C. The caecum with its content and appendix was isolated and weighed. The content of the caecum was collected and kept at -80°C until microbiota and metabolome analysis. A fragment of caecal tissue was collected and placed in cold PBS without Ca^{2+}/Mg^{2+} (ThermoFisher scientific, cat#10010-015) for epithelial cell isolation. Other sections of caecal tissue were fixed in i) Carnoy solution (60% ethanol, 30% chloroform, 10% glacial acetic acid) for 3 hours before transfer in 70% ethanol (samples used for Alcian Blue and Periodic Acid of Schiff staining), or in ii) 10% neutral-buffered formalin for 24 hours before transfer in 70% ethanol (samples used for immunohistochemistry and RNA *in situ* hybridization), or in iii) 0.1 M Sörensen phosphate buffer (pH 7.4) with 2% glutaraldehyde at 4°C (samples used for electron microscopy).

Caecal epithelial cell isolation

Caecal tissue was opened longitudinally and washed with cold PBS to remove all content. The tissue was minced into 1 cm^2 sections and washed with cold PBS. Tissue segments were transferred to 5 mL of a pre-warmed (37°C) digestion solution prepared in HBSS without Ca^{2+}/Mg^{2+} (ThermoFisher Scientific, cat#14175095) and supplemented with 5 mM EDTA (ThermoFisher Scientific, cat#AM9260G) and 1 mM DTT (Sigma, cat# 10197777001). After incubation (20 minutes at 37°C under slow agitation at 15 rpm), epithelial crypts were detached by vigorous manual shaking for one minute. The crypt solution was then filtered (100 µm) before centrifugation (300 × g for 5 minutes at 4°C). The crypt pellet was resuspended in 10 mL of pre-warmed dissociation solution containing TrypLE (ThermoFisher, cat# 1205036) supplemented with 1 mg/mL DNAse I (Sigma, cat # 10104159001), 5 mM $MgCl_2$ (Sigma, cat# M1028), 10 µM Y27632 (StemCell Technologies, cat# 72304) and the solution was distributed in two 50 mL conical tubes (5 mL/tube). Cells were incubated for 10 minutes at 37°C under gentle agitation at 15 rpm before homogenization by vortexing (3 seconds). This step was repeated and followed by two successive filtrations (70 µm and 40 µm). Digestion was stopped by adding 45 mL of cold PBS to the cells. After centrifugation (300 × g for 5 minutes at 4°C), the cells were resuspended in 5 mL FACS buffer (PBS supplemented with 3% fetal bovine serum [ThermoFisher Scientific, cat#10270-106], 2 mM EDTA, and

10 µM Y27632). Cell concentration was measured using an automated cell counter Countess 3 (ThermoFisher Scientific, cat#AMQAX2000).

Cell preparation for single-cell sequencing

Cells (2×10^6) were centrifuged (300 × *g* for 5 minutes at 4°C) and resuspended in 1 mL of PBS supplemented with 10 µM Y27632. This step was repeated twice. Dead cells were stained with the LIVE/DEAD™ Fixable Violet Dead Cell Stain Kit (ThermoFisher Scientific, cat#L34963), according to the manufacturer's instructions. After 30 minutes of incubation (4°C, protected from light), cells were centrifuged (300 × *g* for 5 minutes at 4°C) and resuspended in 1 mL FACS buffer. This step was repeated once. Cells were filtered (40 µM) and sorted (10^5 live and single-cells) in a 1.5 mL tube containing 10 µL of PBS supplemented with 10 µM Y27632 by using a BD Influx cell sorter instrument with a 100 µm nozzle, under 20 psi at the I2MC Cytometry and Cell sorting TRI platform (Toulouse, France). After centrifugation (300 × *g* for 5 minutes at 4°C), cells were resuspended in 100 µL PBS, counted manually and their viability was verified by trypan blue staining.

Single-cell sequencing

For single-cell RNA-sequencing, approximately 10,000 cells per sample were used for encapsulation into droplets using Chromium Next GEM Single-cell 3′ Reagent Kits v3.1 according to manufacturer's protocol (10x Genomics CG000315 Rev E user guide). Briefly, after generation of Gel bead-in-EMulsions (GEMs) using Next GEM Chip G, GEMs were reverse transcribed in a C1000 Touch Thermal Cycler (BioRad) programmed at 53°C for 45 min, 85°C for 5 min, and held at 4°C. After reverse transcription, single-cell droplets were broken and cDNA was isolated and cleaned with Cleanup Mix containing DynaBeads (ThermoFisher Scientific). cDNA was then amplified with a C1000 Touch Thermal Cycler programmed at 98°C for 3 min, 12 cycles of (98°C for 15 s, 63°C for 20 s, 72°C for 1 min), 72°C for 1 min, and held at 4°C. Subsequently, approximately 250 ng of amplified cDNA was fragmented, end-repaired, A-tailed, index adaptor ligated, and cleaned with cleanup mix containing SPRIselect Reagent Kit

(Beckman Coulter, cat# B23317) in between steps. Post-ligation product was amplified and indexed with a C1000 Touch Thermal Cycler programmed at 98°C for 45 s, 11 cycles of (98°C for 20 s, 54°C for 30 s, 72°C for 20 s), 72°C for 1 min, and held at 4°C. The sequencing-ready libraries were cleaned up with SPRIselect beads. 10x libraries were pooled and charged with 1% PhiX on one S1 lane of the NovaSeq 6000 instrument (Illumina) using the NovaSeq 6000 S1 Reagent Kit v1.5 (100 cycles), and the following sequencing parameters: 28 bp read 1 – 10 bp index 1 (i7) – 10 bp index 1 (i5) – 150 bp read 2. The S1 lane generated a total of 810×10^6 raw reads.

ScRNA-seq pre-processing, filtering, normalization and clustering

Cell Ranger Software (version 7.1.0, 10x Genomics) was used to align and quantify raw sequencing data using the rabbit reference genome (GCF_009806435.1_UM_NZW_1.0). A custom reference file was created using the Cell Ranger mkgtf command with "--attribute=gene_biotype:protein_coding and --attribute=gene_biotype:lncRNA" parameters. The Cell Ranger mkref and count commands were used with default parameters.

Using R software (version 4.2.1), the Seurat (version 4.3.0) pipeline (Butler et al. 2018) was run for data preprocessing and analysis. Cells with less than 1,600 or more than 55,000 expressed genes were filtered out. Similarly, cells with a number of counts below 1,500, with a percentage of mitochondrial RNA above 25% or expressing more than 0.1% of counts from hematopoietic cell genes (*CD44, PTPRC, CD48*) were filtered out. The resulting data were normalized via the *NormalizeData* function of Seurat, with the *LogNormalize* method. The top 2,000 variable features were then extracted (based on a mean-variance trend as implemented in the *FindVariableFeatures* function of Seurat). After scaling data to unit variance, dimensionality reduction was carried out with Principal Components Analysis (50 PCs). Cell clustering was performed based on retained PCs and using the Leiden algorithm on a cell similarity graph, with a 0.5 resolution. Finally, clusters were visualized using the non-linear reduction dimensionality Uniform Manifold Approximation and Projection (UMAP) performed on PCA reduction (30 PCs).

Cell type assignment

Marker genes

The marker list for each cluster was obtained using a Wilcoxon test as implemented in the Seurat function *FindMarkers*. A gene was declared a marker if its adjusted *p*-value < 0.05 (Bonferroni correction for multiple testing). The test results were further filtered to ensure a minimum log-Fold Change (logFC) of 0.25 between the tested cluster and the others. Only genes expressed in at least 25% of cells and over-expressed in the tested cluster (compared to the others) were considered for this analysis. Cell types were then manually assigned to clusters according to found markers, based on a comparison with known cell type markers (Parikh et al. 2019; Elmentaite et al. 2021; Burclaff et al. 2022; Wiarda et al. 2023).

Assessment of cluster validity with cell cycle score and crypt axis gene score

The cell cycle score was used to assign phases of the cell cycle to individual cells and assess the consistency between manually assigned cell types and expected cell cycle phase. The cell cycle score was computed with the Seurat function *CellCycleScoring*. In addition, the crypt axis gene (CAG) score of each cell was calculated via the *AddModulesScore* function by averaging the expression of genes previously defined as expressed in epithelial cells located at the crypt top (*PLAC8, CEACAM1, TSPAN1, DHRS9, KRT20, RHOC, PKIB, HPGD*) (Parikh et al. 2019).

Pseudo-time analysis

Considering that absorptive cell (AC) subsets are distinguishable from each other based on their differentiation states, we used a pseudo-time analysis to create AC sub-groups with the monocle3 package (version 3.1). The trajectory of cell types was obtained using the *learn_graph* function on the previously generated UMAP and the pseudo-time of each cluster was calculated based on their projection on the trajectory using the *order_cells* function. The trajectory root was set to be the stem cell cluster. Subsequently, three cell subgroups of AC were delineated based on the pseudo-time distribution, which

was found to be trimodal: cells with a pseudo-time below 2.0 were classified as “Early AC”, those with a pseudo-time between 2.0 and 8.6 were classified as “Intermediate AC”, and cells with a pseudo-time above 8.6 were classified as “Mature AC” (Figures S3A and B). Marker extraction was performed for each assigned cell type, similarly to what was performed for cluster markers and as described in the “Marker genes” section.

Automatic assignation of cell types

To validate our manual annotation, we performed an automatic annotation based on the transfer of labels of a reference to the rabbit caecum epithelial cells (Stuart et al. 2019). Human epithelial cells from the large intestine (Elmentaite et al. 2021) were used as a reference. First, a PCA was performed on the reference dataset to reduce its dimension to the first 30 PCs. Then, *FindTransferAnchors* was used to find similar cells between the rabbit and human datasets, called “anchors”. These anchors were then used by the *MapQuery* function to map the rabbit caecum epithelial cells onto the human epithelial cell space. The reference annotation was then transferred from the reference to the rabbit data and visualized on the UMAP. The results of *MapQuery* were also used in the *MappingScore* function to attribute a score to each rabbit cell. Roughly, this score measures how a cell neighborhood is affected by a mapping to and then back from the reference (a higher score corresponds to a more similar neighborhood).

Biological pathways enrichment

Biological enrichment analysis was performed on marker genes of the cell types using the *enrichGO* function from the *clusterProfiler* (version 4.6.1) package (Yu et al. 2012), with all expressed genes as the reference background. The enrichment analysis was carried out using the *Homo sapiens* database because of the absence of an *Oryctolagus cuniculus* database. Redundancy of results was reduced by using the *simplify* function from the *clusterProfiler* package. Terms with a semantic similarity over 0.7 were deleted and only representative terms (terms with the smallest *p*-value) were kept within each group of term. *p*-values were corrected for multiple testing using the Benjamini-Hochberg (BH) procedure (Benjamini and

Hochberg 1995) and pathways were considered enriched if their corresponding adjusted *p*-value was < 0.05.

Differential analysis of gene expression

The pseudo-counts data were derived by summing the counts of each gene across cells of the same type for each rabbit. This step is considered essential as it has been shown that performing the differential analysis on pseudo-bulk data yields more robust results, reducing the risk of Type I errors compared to analyzing scRNA-seq data directly (Zimmerman et al. 2021; Murphy and Skene 2022). The whole analysis was performed independently in each cell type. Pseudo-counts were normalized using the "TMM" method of e*dgeR* (Robinson et al. 2010). A PCA was conducted on log2-transformed pseudo-counts for quality control, revealing a possible important impact of the litter on gene expression (Figure S4). This was thus accounted for in the differential analysis. Differential expression analysis was performed using a Negative Binomial generalized linear model as implemented in *edgeR*. More precisely, each gene expression was modeled with an additive effect of both the group and the litter, the latter being used as a blocking variable. *p*-values were obtained with a log-likelihood ratio (LR) test of the group effect. Adjusted *p*-values were obtained with the BH procedure and genes were considered differentially expressed if their corresponding adjusted *p*-value was < 0.05. Differentially expressed genes were subjected to an enrichment analysis as described in the "Biological pathways enrichment" section.

Microbiota composition

The microbiota composition was analyzed as described previously (Beaumont et al. 2020). Briefly, DNA was extracted from 50 mg of caecal content with the Quick-DNA Fecal/Soil Microbe DNA Miniprep Kit (Zymo Research, cat#D6010). The V3-V4 region of the 16S gene was amplified by PCR and amplicons were sequenced by MiSeq Illumina Sequencing. Bioinformatic analyses were performed with the FROGS pipeline (v.4.0.1) according to the guidelines (Escudié et al. 2018). Taxa representing more than 0.5% of

the relative abundance in at least one group were considered for analysis, as it was previously shown that taxa below this threshold were not accurately quantified (Paës et al. 2020).

Metabolomics

The metabolome was analyzed in 50 mg of caecal content by using nuclear magnetic resonance (NMR)-based metabolomics, at the MetaboHUBMetaToul-AXIOM metabolomics platform (GenotToul, Toulouse, France), as described previously (Beaumont et al. 2020). The relative concentration of each metabolite was expressed relatively to the mean quantification measured in the Milk group.

Plasma biochemistry

The Clinical Chemistry Analyzer Pentra C400 (Horiba medical) was used at the Anexplo Phenotyping platform (GenoToul, Toulouse) to measure plasmatic concentrations of cholesterol, high density lipoprotein (HDL), low density lipoprotein (LDL), glucose, triglycerides, free fatty acids and urea.

Calprotectin assay

Caecal epithelial cells isolated as described above were lysed in RIPA buffer (ThermoFisher Scientific, cat#89901) supplemented with cOmplete protease inhibitor cocktail (Roche, cat#11697498001) by using stainless steel beads and a TissueLyser II (Qiagen) operating at 30 Hz for 3 min. Lysates were centrifuged (12000 × g, 10 min, 4°C) and stored at -80°C until analysis. Calprotectin was quantified in undiluted epithelial cell lysates by using a rabbit-specific ELISA kit (Clinisciences, cat# MBS2601529-48), following the manufacturer instructions. Protein concentration in epithelial cell lysates diluted 1:2 (v/v) in NaCl 0.9% was measured with Pierce Bradford Plus Protein Assay Kits (ThermoFisher Scientific, cat#23236). Calprotectin concentration was normalized to the protein level of each sample.

Histology

Transversal sections of cecal tissue with luminal content fixed in Carnoy's solution were embedded in paraffin and stained by Alcian Blue and Periodic Acid of Schiff at the histology platform Anexplo (GenoToul, Toulouse, France). Slides were digitalized before measurement of the crypt depth and of the number of goblet cells per crypt with the CaseViewer 2.3 software (3DHISTECH). Formalin-fixed, paraffin-embeded (FFPE) transversal sections of cecal tissues were cut into 4 µm sections and adhered to Superfrost-Plus charged microscope slides (Thermo Fisher Scientific) before being used for RNA *in situ* hybridization and immunohistochemical staining.

RNA in situ hybridization

The RNAscope 2.5 HD Reagent Kit – RED (Advanced Cell Diagnostics, cat#322350) and the RNAscope Multiplex Fluorescent Reagent Kit v2 (Advanced Cell Diagnostics, cat#323100) were used with rabbit custom probes targeting *SPINK4* (Advanced Cell Diagnostics, cat#1564251-C1, RNAscope™ Probe- Oc-SPINK4-C1) or *BEST4* (Advanced Cell Diagnostics, cat#1564261-C1, RNAscope™ Probe- Oc-BEST4-C1) or *PIGR* (Advanced Cell Diagnostics, cat#1003001-C1, RNAscope™ Probe- Oc-PIGR-C1). Negative and positive control slides were respectively hybridized with the RNAscope™ Negative Control Probe-DapB (Advanced Cell Diagnostics, cat#310043) and RNAscope™ Probe- Oc-GAPDH-No-XHs (Advanced Cell Diagnostics, cat# 469461) or RNAscope™ Probe- Oc-POLR2A (Advanced Cell Diagnostics, cat# 410571).

The chromogenic assay (*SPINK4*) was performed as described before with minor modifications (Palmer et al. 2019). Briefly, slides were incubated at 60°C to enhance tissue adherence. Slides were deparaffinized using xylene and rehydrated through a series of graded ethanol washes. Slides were treated with hydrogen peroxide to block endogenous peroxidase activity, followed by epitope unmasking using a boiling target retrieval solution. Hydrophobic barriers were drawn around the tissues to contain reagents. Unless stated otherwise, all incubations were performed at 40°C in a HybEZ hybridization oven followed by a 1x Wash

Buffer wash. Slides were incubated with the Protease Plus for 15 minutes to break down RNA-associated proteins. Probes were then applied to each slide and incubated for 2 hours. The amplification steps were carried out sequentially using AMP1, AMP2, AMP3, AMP4, AMP5, and AMP6, with varying incubation times (30, 15, 30, 15, 30, and 15 minutes) and temperatures (40°C for AMP1–4, and room temperature for AMP5 and AMP6). Chromogenic detection was performed using a 1:60 dilution of RED-A:RED-B, followed by a counterstaining with Gill's Hematoxylin I (American Master Tech Scientific, cat# HXGHE1LT, diluted 1:1 in dH□O). Slides were immediately air-dried for 20 minutes at room temperature, after which two drops of Vecta Mount (Vector Laboratories, cat# H-5700-60) were applied. Coverslips (#1 thickness) (Fisherbrand, cat# 12-545-F) were mounted, and the slides were left to dry for 20 minutes at room temperature.

The fluorescent *in situ* hybridization (*PIGR* and *BEST4*) assay was performed identically to the chromogenic assay for the pretreatment and the hybridization steps. The amplification was performed with AMP1 (30 minutes), AMP2 (15 minutes), and AMP3 (15 minutes). Detection was performed with horseradish peroxidase channel 1 (HRP-C1) for 15 minutes and washed. The Opal 570 Reagent fluorophore (Akoya Biosciences, cat#FP1488001KT, dilution 1:750 in RNAscope Multiplex TSA Buffer [Advanced Cell Diagnostics, cat# 322809]) was incubated on the slides for 30 minutes. After the wash, the horseradish peroxidase (HRP) blocker was added to the slides and incubated for 15 minutes. Similarly to the chromogenic assay, incubations were performed at 40°C in a HybEZ oven, followed by a wash performed twice with 1X Wash Buffer for 2 minutes at RT. All the slides were incubated with DAPI (Advanced Cell Diagnostics, cat# 323108) for 30 seconds at RT and mounted with 2 drops of ProLong Gold Antifade reagent (Invitrogen, cat# P36930) and covered with #1.5 thickness cover glass (Fisherbrand, cat# 12-545-F).

Chromogenic immunohistochemistry (IHC)

The IHC assay was performed as described before (Wiarda et al. 2020). Briefly, slides were incubated for 20 minutes at 60°C, deparaffinized in xylene, and rehydrated with ethanol and distilled water using a histological automaton (Leica Biosystem, cat#ST5020). Antigen retrieval was performed by submerging the slides in preheated distilled water, followed by incubation in 1X sodium citrate solution for 15 minutes at 95°C. Hydrophobic barriers were drawn around the sections, and slides were incubated with Dual Endogenous Enzyme Block (Dako, cat#S2003) for 10 minutes at RT, Protein Block (Dako, cat#X0909) for 20 minutes at RT, and primary antibody ([Goat Anti-Rabbit IgA, Abcam Limited, cat#ab97186, 1:3000], [Mouse anti-KI67, BD Biosciences, cat#AB_393778; 1:40], dilution in 1% bovine serum albumin [BSA] PBS, 4°C overnight) sequentially. Slides were then incubated with a secondary antibody ([ImmPRESS™ HRP Anti-Goat Ig, Vector, cat# MP-7405] or [HRP Labelled Polymer Anti-Mouse, Dako, cat#K400111-2]) for 30 minutes at RT, followed by DAB chromogen for 7 minutes at RT in the dark, and counterstained with 25% diluted Gill's hematoxylin (American Master Tech Scientific, cat#HXGHE1LT) for 1 minute at RT. Slide washes were performed after each incubation using a 0.05% PBS-Tween solution. Slides were dehydrated in ethanol and Propar clearant (Anatech, cat#510) sequentially, mounted with Refrax Mounting Medium (Anatech, cat#711), and covered with #1 thickness cover glass (Fisherbrand, cat#12-545-F) using a histological automaton (Leica Biosystem, cat#ST5020). Negative controls were treated with 1% BSA in PBS without the primary or secondary antibodies.

Electron microscopy

Electron microscopy analyses were performed in CMEAB (Toulouse, France). *Transmission electron microscopy (TEM):* Following fixation, samples were washed overnight in 0.2 M Sörensen phosphate buffer (pH 7.4). Post-fixation was carried out at room temperature for 1 hour in 0.05 M Sörensen phosphate buffer (pH 7.4) with 1% OsO_4 and 0.25 M glucose. Dehydration was performed using graded ethanol series at room temperature, up to 70%. From then, the tissues were embedded in Embed 812 resin (Electron Microscopy Sciences) using a Leica EM AMW automated microwave tissue processor for electron microscopy. Once poylymerized, the samples were sliced into ultrathin sections (70 nm) using an

Ultracut Reichert Jung ultramicrotome and mounted onto 100-mesh Formvar-coated copper grids. Sections were then stained with 3% uranyl acetate in 50% ethanol and Reynold's lead citrate. Examinations were conducted on a transmission electron microscope (Hitachi HT7700) at an accelerating voltage of 80 kV. *Scanning electron microscopy (SEM):* After washing the sample in water, dehydration was performed through a graded ethanol series, up to 100% ethanol. Critical point drying was carried out with a Leica EM CPD 300. Dried samples were then coated with a 6 nm layer of platinum using a Leica EM MED020. SEM imaging was performed using a FEG FEI Quanta 250 scanning electron microscope at an accelerating voltage of 5 kV.

Statistical analyses of microbiota, metabolites and calprotectin data

Statistical analyses of the log transformed relative abundances of bacterial taxa and metabolite concentrations (caecum or plasma), and calprotectin concentration in epithelial cells were analyzed with the R software (version 4.2.1). Linear mixed models were used with the group as a fixed effect and the litter as a random effect. *p*-values were corrected for multiple testing using the BH procedure. The significance of the group effect was tested and results were considered significant if their corresponding adjusted *p*-value was < 0.05.

Data availability

The scRNA-seq data for this study have been deposited in the European Nucleotide Archive (ENA) at EMBL-EBI under accession number PRJEB74645 (www.ebi.ac.uk/ena/browser/view/PRJEB74645). The data are also accessible on the FAANG portal (www.data.faang.org/dataset/PRJEB74645) and are publicly available on the Broad Institute Single-cell Portal (https://singlecell.broadinstitute.org/single_cell/study/SCP2662/single-cell-transcriptomics-in-caecum-epithelial-cells-of-suckling-rabbits-with-or-without-access-to-solid-food). 16S sequencing data have been deposited in NCBI Sequence Read Archive (SRA) under accession number PRJNA1130383. NMR raw spectra have been deposited in Metabolights under accession number MTBLS10648.

Results

To evaluate the effects of solid food introduction on epithelial maturation, we determined single-cell transcriptomic profiles of caecal epithelial cells isolated from age-matched littermate suckling rabbits ingesting or not solid food (Milk group: n = 4, Milk+Solid group: n = 4, Figure S1A). Growth and milk intake were similar in the two groups (Figures S1B and C). In the Milk+Solid group, the small amount of solid food ingested (< 25g/day/rabbit) increased dramatically the weight of the caecum (Figures S1D and E).

A single-cell atlas of the rabbit gut epithelium

After applying quality filters and removal of hematopoietic cells, the dataset included 13,805 caecal epithelial cells (Figures S2A-E). We identified 13 clusters of cells based on their transcriptome profiles (Figures S2F-G). Each cluster was assigned to a cell type based on expression of known markers of epithelial lineages (Figures 1A-C, Figure 2A and Table S1), pseudo-time analysis (Figure 1D, Figure S3A and B) and cell cycle score (Figure 1E). The proportion of each cell type was calculated to determine if it was consistent with the literature (Figure 2C). Crypt position score (Figure 2B), enriched biological processes (Figure 2D, Table S2), and automatic annotation (Figure S3C) were used as quality controls for our manual annotation. Tables S1 and S2 respectively provide the lists of marker genes and of enriched biological processes, for each cell type.

Stem (*LGR5*$^{+}$, 7% of epithelial cells) and transit amplifying (TA) cells (*MKI67*$^{+}$, *TOP2A*$^{+}$, *UBE2C*$^{+}$, 8.8% of epithelial cells) were predicted to be positioned at the crypt base (Figures 1B-C, Figures 2A-C). Immunodetection of Ki67 (encoded by *MKI67*) confirmed that TA cells were localized at the crypt base (Figure 1F). Stem and TA cells were predicted in the S and G2M cell cycle phases, respectively, while most other epithelial cells were in the G1 phase (Figure 1E). Both stem and TA cells expressed high levels of genes involved in DNA replication and translation (Figure 2D). TA cells specifically expressed genes related to mRNA processing and nuclear division (Figure 2D). Absorptive cells (*SLC51B*$^{+}$) were the main

epithelial cell population and the distribution of their pseudo-times indicated three main differentiation states that we termed as early (15.3% of epithelial cells), intermediate (30.9% of epithelial cells) and mature (23.5% of epithelial cells) (Figures 1C-D, Figure 2C and Figures S3A-B). Absorptive cell gene expression profiles showed gradual modifications according to their differentiation states, which reflect their maturation during migration along the crypt axis (Figure 2A). Indeed, early absorptive cells were predicted to be localized at the lower part of crypts, while mature absorptive cells were positioned at the crypt-top (Figure 2B). Gene expression profile of early absorptive cells was intermediate between stem/TA cells and other absorptive cells (Figure 1B and Figure 2A). Intermediate absorptive cells expressed high levels of genes involved in antimicrobial defenses (e.g., *S100A8, S100A12, DMBT1*) and in mitochondrial metabolism (Figure 1B, Figures 2A and D, Table S1 and Table S2). Mature absorptive cells highly expressed genes involved in epithelial digestion, transport, and glycocalyx formation (e.g., *CA1, AQP8, ABCA1, APOB, ANPEP, MUC12*) (Figure 1B, Figure 2A and Table S1), and genes involved in lipid metabolism, response to hypoxia, and antimicrobial defenses (Figure 2D and Table S2).

BEST4$^+$ cells (5% of epithelial cells), a recently discovered subset of mature absorptive epithelial cells, were identified by the expression of the canonical markers *BEST4, CA7, OTOP2, GUCA2B, GUCA2A,* and *CFTR* (Figures 1B and C, Figures 2A and 2C and Table S1). BEST4$^+$ cells were predicted to be distributed along the crypt axis (Figure 2B). *BEST4* mRNA *in situ* hybridization confirmed that BEST4$^+$ cells are relatively rare (< 4 BEST4$^+$ cells per crypt) and distributed along the crypt axis (Figure 1G). Functions enriched in BEST4$^+$ cells included “regulation of exocytosis” and “intracellular pH reduction” (Figure 2D and Table S2). Although the morphological features of BEST4$^+$ cells are not defined yet, we observed rare electron dense absorptive cells and cells with low density microvilli that may correspond to distinct subsets of absorptive epithelial cells (Figures 1I-i and ii).

Goblet cells (6.9% of epithelial cells) were identified by expression of known markers of this lineage and of major components of mucus (*SPINK4, REG4, FCGBP, WFDC2, AGR2, ZG16, TFF3*) (Figures 1B and

C, Figure 2A and C and Table S1). Goblet cells were predicted to be distributed across the crypt axis (Figure 2B) and we confirmed their localization by *SPINK4* mRNA *in situ* hybridization (Figure 1H). Genes specifically expressed by goblet cells were involved in "glycosylation" and "Golgi organization" (Figure 2D and Table S2), which reflects their role in the synthesis of mucins, also illustrated by goblet cells morphological features (Figures I-iii and iv). Enteroendocrine cells (EEC) (*CHGA*$^+$, *NEUROD1*$^+$) specifically expressed genes involved in the secretion of hormones (Figures 1C and Figure 2A, Tables S1 and S2). Two subclusters of EEC were distinguished based on their repertoire of hormone-related genes. EEC CHGB$^+$ (2.2% of epithelial cells, enterochromaffin-like cells) expressed *TAC1*, *TTR*, *NMU*, and *TPH1* whereas EEC PYY$^+$ (0.4% of epithelial cells, L-like cells) expressed *GCG*, *MLN*, and *CCK* (Figure 1B, Figure 2A and Table S1). Electron microscopy confirmed the presence of rare enteroendocrine cells containing electron dense granules at the basal side (Figure I-v).

Other rare cell types described in the intestinal epithelium of other species (tuft cells, Paneth cells, M cells) were not found in our rabbit gut scRNA-seq dataset. However, we observed at the base of epithelial crypts a few Paneth-like cells containing electron dense apical granules, whose scarcity and/or sensitivity to microfluidic flow may preclude their capture in droplets (Figure 1I-vi). Automatic cell annotation based on human large intestine scRNA-seq data was consistent with the manual assignment of cell types (Figure S3C). The mapping score indicating the degree of similarity between rabbit and human cells was the highest for stem cells, TA cells, BEST4$^+$ cells, mature absorptive cells and for subsets of goblet and enteroendocrine cells (Figure S3D). All cell types were identified in each rabbit (Figure S3E). In sum, our analysis provided the first single-cell transcriptomic atlas of the rabbit intestinal epithelium. We have made these gene expression data available as a searchable tool on the Broad Institute Single-cell Portal (https://singlecell.broadinstitute.org/single_cell/study/SCP2662/single-cell-transcriptomics-in-caecum-epithelial-cells-of-suckling-rabbits-with-or-without-access-to-solid-food#study-visualize).

Solid food introduction induced both global and cell type specific transcriptomic modifications in the intestinal epithelium

After characterizing the cellular diversity of the rabbit intestinal epithelium, we focused our analysis on the effects of solid food introduction on gene expression in each epithelial cell type. Ingestion of solid food altered the transcriptome of absorptive cells, as suggested in the UMAP by the low overlap between absorptive cells from suckling rabbits ingesting or not solid food (Figure 3A). Accordingly, the highest number of differentially expressed genes (DEG) was found in intermediate and mature absorptive cells with 890 and 868 DEG, respectively (Figures 3B-D, Figure S4). Although to a lesser extent, solid food introduction also modified the transcriptome in BEST4^{+} cells (429 DEG), early absorptive cells (268 DEG), TA cells (209 DEG), goblet cells (198 DEG), stem cells (189 DEG), EEC PYY^{+} (54 DEG), and EEC CHGB^{+} (41 DEG) (Figures 3B-D). These solid food induced alterations of gene expression were observed despite the proportion of epithelial cell types remaining similar in the two groups (Figure 3C). Table S3 provides the list of DEGs for each cell type. Table S4 contains the results of the enrichment analysis using DEGs of each cell type. All the biological functions and genes cited below were significantly modulated following the introduction of solid food (adjusted p-value < 0.05).

Most of the modifications of gene expression induced by the introduction of solid food were cell type specific while other changes were shared between cell types (Figure 3D). Notably, mature absorptive cells and BEST4^{+} cells shared a high number of DEG (Figure 4A). Among transcriptomic modifications shared between most cell types, solid food introduction induced a strong upregulation of *ALDH1A1*, encoding an enzyme involved in retinoic acid metabolism, and an upregulation of *CA1*, a typical marker of epithelial differentiation in the large intestine (Figures 4B-D). Solid food introduction also increased the gene expression of the immunoglobulin transporter *PIGR* in several cell types, and this effect was much more pronounced in cells located at the bottom of the crypts (Figures 4B and E). *PIGR* mRNA *in situ* hybridization confirmed its predominant expression at the base of epithelial crypts (Figure 4F). The expression of *PIGR* was also increased by solid food ingestion in goblet cells that were found to contain

immunoglobulin A (IgA) (Figures 4E and G). Among the cell type specific modifications, solid food ingestion reduced the gene expression of *LRIG1*, a master regulator of the stem cell niche, exclusively in stem cells (Figure 4B). Conversely, ingestion of solid food upregulated the gene expression of the transcellular water transporter *AQP8*, mostly in mature absorptive cells (Figure 4B and H). In BEST4$^+$ cells, solid food introduction increased the expression of the pH-sensitive ion channel *OTOP2*, while it reduced the expression of the interleukin *IL33* (Figures 4B, I, and J). Overall, our results showed that the introduction of solid food induced major transcriptomic modifications in the intestinal epithelium of suckling rabbits and these changes are either shared across cell types or cell type specific. Accordingly, enrichment analyses revealed that solid food ingestion altered specific functions in every epithelial cell type (Figure 4K and Table S4).

Solid food introduction remodels defense systems in the intestinal epithelium

Solid food introduction upregulated the expression of genes involved in detoxification in all cell types, except EEC (e.g., *GPX2, GSTO1, GSTP1, MGST1, MGST3, SOD1, TXN*) (Figure 5A). This was particularly marked in intermediate and mature absorptive cells, and in BEST4$^+$ cells. This finding is linked to the enrichment of biological pathways related to “cellular aldehyde metabolic process”, “response to toxic substance”, and “response to oxidative stress” in absorptive cells and in BEST4$^+$ cells (Figure 4K). Solid food ingestion also increased the expression of interferon-stimulated genes (ISG), primarily in mature absorptive cells and BEST4$^+$ cells (e.g., *DHX58, OASL, IFIT3, IFI35, IFI44L, IRF9, MX1, USP18, RIGI*) (Figure 5B), which is consistent with the specific enrichment of biological pathways such as “response to virus” and “defense response to symbiont” in these cell types (Figure 4K). Conversely, solid food ingestion decreased the expression of several genes coding for regulators of innate immune responses in absorptive cells (e.g., *AREG, NFKBIA, NFKBIZ*) (Figure 5C). This was associated with a cell type-specific downregulation of genes coding for cytokines in BEST4$^+$ cells (*CXCL9, IL13RA1, IL33*), which were also characterized by a specific enrichment of the biological pathway “negative regulation of cytokine production” (Figure 4K). Other cell type specific downregulations of

cytokine gene expression induced by solid food ingestion included *IL1A* in mature absorptive cells and *CCL25* in stem and early absorptive cells. In contrast, solid food introduction upregulated the expression of other cytokines expressed by small subsets of absorptive and BEST4$^+$ cells (e.g., *IL18, IL32, IL34*) (Figure 5C). Solid food reduced the expression of some antimicrobial peptides in mature absorptive cells (*DMBT1* and *DEFB1*) and in goblet cells (*WDFC2*) while increasing the expression of numerous antimicrobial proteins of the S100 family in several cell types (e.g., *S100A1, S100A12, S100A14, S100A6, S100G*) (Figure 5D). Interestingly, genes coding for the two subunits of the inflammation marker calprotectin (*S100A8/S100A9*) were upregulated, notably in subsets of stem and TA cells (Figure 5D). The increased expression of calprotectin by epithelial cells after the ingestion of solid food was confirmed at the protein level in an independent experiment (Figure 5E).

Solid food introduction also modulated the expression of numerous genes involved in epithelial glycosylation, which plays a key role in host-microbiota interaction. Solid food decreased the expression of several genes coding for glycosyltransferases mostly in stem, TA, early absorptive and goblet cells (e.g., *GALNT13, GALNT18 ST3GAL5, ST6GAL1, ST6GAL2*) while *B4GALT1* was upregulated in mature absorptive and BEST4$^+$ cells (Figure 6A). In contrast, the introduction of solid food increased the expression of genes coding for fucosyltransferases (*FUT2* and *FUT9*) which are expressed by subsets of absorptive cells (Figure 6A). The introduction of solid food also altered the expression of genes related to mucin production (Figure 6B). Specifically, solid food ingestion reduced the expression of genes encoding the glycocalyx-forming transmembrane mucins *MUC1* and *MUC13* in intermediate and mature absorptive cells, while enhancing *MUC12* expression in BEST4$^+$ cells (Figure 6B). In goblet cells, the expression of genes coding for major mucus components were upregulated (e.g., *TFF1, TFF2, ZG16*) or downregulated (e.g., *BCAS1, SYTL2*) after the introduction of solid food (Figure 6B). Histological observations confirmed that the number of goblet cells per crypt was similar in the caecal epithelium of rabbits ingesting or not solid food (Figures 6C-D), which is consistent with the goblet cell proportion estimation obtained by scRNA-seq (Figure 3C).

In order to determine whether changes in the expression of genes involved in epithelial defenses were linked to a change in the microbiota, we performed 16S rRNA gene sequencing in rabbit caecal contents (Table S5). Solid food ingestion by suckling rabbits altered the composition of the microbiota, in particular by increasing the abundance of the *Lachnospiraceae* family (14.6% in the Milk group versus 21.2% in the Milk+Solid group). Altogether, our results show that the introduction of solid food triggered major adaptations of epithelial defense systems in most cell types, which were associated with an alteration of the microbiota composition.

Solid food introduction enhances differentiation in intestinal epithelial cells and alters nutrient handling

As a next step, we evaluated how solid food ingestion altered the expression of genes related to epithelial differentiation (Figure 6E) and renewal (Figure 6F). Key genes involved in stemness and proliferation were upregulated (e.g., *CDKN3, CKS1B, MKI67, OLFM4*) or downregulated (e.g., *CDK14, CELF2, DACH1, LGR5, LRIG1*) in stem cells after the introduction of solid food (Figure 6F). These changes at the gene expression level were not associated with a modification of the crypt depth, which is partly determined by epithelial proliferation rate (Figures 6C and G). In contrast, solid food ingestion strongly increased the expression of the differentiation markers *PLAC8* and *CA1* in most of epithelial cells (Figure 6E). Moreover, the solid food induced upregulation of *AQP8* in mature absorptive cells was associated with the enrichment of the biological pathway “regulation of epithelial cell differentiation” (Figures 4K and 6E). Conversely, in mature absorptive cells, solid food introduction downregulated the expression of *ANPEP*, an enzyme involved in peptide digestion, which is a process usually occurring in the small intestine (Figure 6E). Accordingly, automatic annotation of cell types identified a population of enterocyte-like cells in the group of exclusively suckling rabbits (Figure S3C).

These results suggesting a rewiring of absorptive cell functions after solid food introduction were associated with the modulation of the expression of numerous genes involved in lipid handling and chylomicron biogenesis, mostly in absorptive cells (Figure 7A). These genes were either downregulated (*ABCA1, APOB, PLIN2, VLDR*) or upregulated (*ACAT2, APOM, LDLR)* (Figure 7A). Accordingly, absorptive cell DEGs were enriched in functions related to “lipid transport”, “lipid homeostasis”, and “cholesterol metabolic process” (Figure 4K). Moreover, solid food ingestion increased the expression of several bile acid transporters, such as *FABP7* that was upregulated in most cell types, *FABP6* that was specifically upregulated in BEST4$^+$ cells, and *SLC51A* and *SLC51B* that were mostly upregulated in absorptive cells (Figures 7A and B). These alterations of the expression of lipid processing genes were coupled with an important decrease in the plasmatic concentration cholesterol and LDL after solid food introduction (Figure 7D).

In addition, the introduction of solid food altered the expression of numerous genes coding for SLC carriers (Figure 7B). Ingestion of solid food strongly upregulated the expression of genes coding for the urea transporter *SLC14A2* and several ion transporters (e.g., *SLC11A2, SLC22A18, SLC26A3, SLC39A4)* in absorptive cells (Figure 7B). The upregulation of the urea transporter coincided with a significant decrease in plasma urea concentration following the introduction of solid food (Figure 7D). Solid food ingestion also specifically upregulated the ion transporter *SCL12A7* in BEST4$^+$ cells and the fucose transporter *SLC35C1* in goblet cells. The introduction of solid food altered the expression of monocarboxylic transporters with an upregulation of *SLC16A9* in mature absorptive cells and a downregulation of *SLC16A3* in BEST4$^+$ cells and of *SLC16A7* in early absorptive cells (Figure 7B). This result can be linked to the increased concentrations of the bacterial short chain fatty acids acetate and butyrate in the caecum content after the introduction of solid food (Figure 7E). Similarly, the lower concentration of amino acids (glutamate, methionine, and tyrosine) following solid food introduction could be linked to the upregulation (*SLC38A3)* and downregulation (*SLC38A2, SLC6A14, SLC7A1*) of amino acids transporters in absorptive cells (Figures 7B and 7E).

The solid food-induced alterations of nutrient handling were associated with modifications of gene expression in EEC (Figure 7C). In EEC PYY^{+} cells, solid food introduction upregulated the expression of genes coding for the hormones *GHRL*, *MDK*, *MLN*, *SST*, *PPY*, and *TAC1*, while only *NTS* was downregulated. In *EEC CHGB*$^{+}$, solid food ingestion increased the expression of the hormone coding gene *NMU*, while *TTR* was downregulated (Figure 7C). These observations are reflected by the EEC-specific enrichment of DEG involved in the biological pathway "digestion" (Figure 4K). In addition, genes coding for the hormones involved in the guanylate cyclase C signaling (*GUGA2A* and *GUCA2B*) were upregulated in goblet cells, mature absorptive cells and BEST4^{+} cells (Figure 7C). Overall, our results show that solid food ingestion enhances epithelial differentiation and remodels the sensing, transport and metabolism of nutrients by epithelial cells.

Discussion

Our study provides the first single-cell transcriptomic atlas of the rabbit intestinal epithelium. This dataset expands the characterization of the cellular diversity of the intestinal epithelium in mammals and constitutes an important resource for the use of rabbits as a model in gastrointestinal research. Our results notably highlighted the diversity of absorptive epithelial cells in the caecum. Indeed, we observed a functional specialization of absorptive cell subsets along the caecal crypt axis that mirrored previous findings in the small intestine villi (Moor et al. 2018; Beumer et al. 2022). For instance, our results showing that middle-crypt absorptive cells specifically express genes coding for antimicrobial peptides is consistent with the observation made in bottom villus enterocytes (Moor et al. 2018; Beumer et al. 2022). Another important finding of our study is the high homology between rabbit and human BEST4^{+} cells, which suggests that the rabbit could be an appropriate animal model to study the role of this subset of mature absorptive cells that are absent in mice (Malonga et al. 2024). Additionally, the two subsets of EEC that we identified in the rabbit caecum (EEC PYY^{+}, corresponding to L-cells expressing *GCG* and *PYY*; EEC CHGB^{+}, corresponding to enterochromaffin cells expressing *TPH1*) were highly similar to human EEC, notably because EEC from both species express the hormones *MLN*, *MDK*, and *PPY* which are not expressed by mouse EEC (Parikh et al. 2019; Beumer et al. 2020). The absence of M cells in our caecal epithelium dataset was expected as these cell types are known to be present only in the small intestine (Burclaff et al. 2022; Schumacher 2023). The lack of Paneth and tuft cells in our single-cell survey could be explained by their scarcity, which reduces their probability of capture by droplets in the microfluidic system (Silverman et al. 2024). Indeed, our electron microscopy observations revealed a rare population of Paneth-like cells in rabbit caecal epithelial crypts, confirming previous reports (Cui et al. 2023).

The maturation of the intestinal epithelium at the suckling-to-weaning transition is considered to be largely driven by genetically wired factors while the contribution of nutritional and microbial signals remains debated (Muncan et al. 2011; Navis et al. 2019; Beaumont et al. 2022; Díez-Sánchez et al. 2024).

Our results clearly demonstrate that the introduction of solid food is sufficient to induce major transcriptome modifications in every intestinal epithelial cell type, independently of age-related factors. Importantly, we observed this strong epithelial response to solid food despite the level of milk intake remaining unchanged, which indicates that the loss of milk-derived factors is not mandatory to induce epithelial maturation. Several previous studies described the transcriptomic changes occurring in the intestinal epithelium at the suckling-to-weaning transition (Rakoff-Nahoum et al. 2015; Pan et al. 2018) but, to our knowledge, our study is the first to reveal in which cell types these modifications take place. For instance, we newly demonstrated that the well characterized up-regulation of the immunoglobulin transporter *PIGR* at the onset of solid food ingestion (Jenkins et al. 2003; Rakoff-Nahoum et al. 2015; Beaumont et al. 2020) mainly occurs in epithelial cells localized at the crypt base (stem cells, TA cells, and early absorptive cells). This zonated expression of *PIGR* in crypt base cells that we confirmed by RNA *in situ* hybridization could be explained by the proximity with the underlying IgA secreting plasma cells. IgA secretion by crypt base cells could contribute to protect the stem cell niche from microorganisms. In line with our findings, the compartmentalization of *PIGR* expression in the intestinal epithelium was recently demonstrated to be driven by BMP signaling, which increases from the crypt base to the top (Beumer et al. 2022). Interestingly, we also observed an upregulation of *PIGR* expression in goblet cells after the ingestion of solid food, which suggests that transepithelial transport of IgA could be an unexplored function of mucus secreting cells. The presence of IgA in rabbit caecal goblet cells, as observed previously in the intestine of birds (Bar-Shira et al. 2014), could be explained by the binding of IgA to mucins or their transport through goblet cell-mediated passage (Knoop and Newberry 2018). Future research is required to explore the potential contribution of goblet cells to IgA transport across the intestinal epithelium.

Although our results indicate that most transcriptome changes induced by solid food ingestion are cell type-specific, we also found a few genes similarly regulated in most epithelial cell types. A striking example is the pan-epithelial upregulation of *ALDH1A1*, which is involved in epithelial processing of

dietary vitamin A into retinoic acid (Bang 2023). Epithelial retinoic acid metabolism was previously shown to be upregulated at the weaning transition in the mouse intestine (Layunta et al. 2021) and is known to be influenced by the gut microbiota (Bang 2023), notably through the bacterial metabolite butyrate, which is able to induce *ALDH1A1* expression in epithelial cells (Schilderink et al. 2016). Accordingly, we observed that the solid food induced upregulation of *ALDH1A1* coincided with an increased concentration of butyrate and a higher abundance of the butyrate-producing family *Lachnospiraceae* (Vacca et al. 2020), which is probably driven by the introduction of plant-based complex carbohydrates. Given the role of retinoic acid in tuning intestinal immune responses (Hall et al. 2011), our results suggest that epithelial regulation of vitamin A metabolism at the onset of solid food ingestion may contribute to the "weaning reaction", which corresponds to a transient remodeling of mucosal immunity essential to program mucosal health (Al Nabhani et al. 2019). In our study focusing on the epithelial layer, we found that a prominent feature of this "weaning reaction" was the strong upregulation of ISG, which was previously shown to be a microbiota-dependent process (Rakoff-Nahoum et al. 2015). Our study newly shows that this solid food induced upregulation of ISG is mostly restricted to crypt-top mature absorptive cells and to BEST4^{+} cells. This observation is in line with previous studies in mice showing that microbial colonization induced the upregulation of ISG specifically in subsets of mature absorptive cells localized at the tip of epithelial villi (Sommer et al. 2015; Van Winkle et al. 2022). In contrast with the upregulation of ISG, we found that solid food ingestion reduced the expression of numerous cytokines and antimicrobial peptides in a cell type specific manner, indicating an overall remodeling of epithelial defense systems. For instance, our data revealed that BEST4^{+} cells are the main producers of the immunomodulating *IL33* alarmin (Schiering et al. 2014), which is downregulated after ingestion of solid food. We also confirmed the goblet cell-specific expression of the recently discovered antimicrobial peptide *WFDC2* (Parikh et al. 2019) and we newly report its downregulation after the introduction of solid food.

Our results showing that solid food ingestion alters the gene expression of membrane mucins (*MUC1, MUC13, MUC12*), specifically in absorptive and BEST4^{+} cells highlight the cell types involved in the establishment of the glycocalyx, which was previously shown in mice to be part of an adaptation of the epithelial defense repertoire during weaning (Layunta et al. 2021). In addition, we found that several glycosyltransferases involved in the post-translational modification of mucins were regulated by the introduction of solid food predominantly in stem cells and proliferating cells located at the crypt-base. This effect may be driven by the changes in the gut microbiota induced by solid food ingestion since a previous study showed that microbial colonization of the mouse intestine similarly changed glycosylation in stem and transit-amplifying cells (Tsang et al. 2022). The mature absorptive cell-specific upregulation of the fructosyltransferase *FUT2* induced by the ingestion of solid food could also be driven by microbial signals but also by changes in glucocorticoid levels at the weaning transition (Nanthakumar et al. 2013; Arike et al. 2017). The solid food induced upregulation of mucus components secreted by goblet cells (*ZG16, TFF2*) could contribute to protect the intestinal epithelium from microorganisms expanding in the gut at the weaning transition.

The remodeling of epithelial defense systems induced by the introduction of solid food coincided with a shift of the transcriptome of caecal epithelial cells characterized by a reduced expression of small intestine-specific genes (*ANPEP, APOB*) and a higher expression of large intestine-specific genes (*AQP8, CA1, SLC26A3*) (Burclaff et al. 2022). The changes in the gut microbiota induced by solid food ingestion could contribute to the acquisition of these large intestine-specific functions since microbial colonization of the rat intestine was previously shown to induce similar effects (Tomas et al. 2015). The regional specialization of epithelial cells upon solid food introduction was associated with a strong shift in amino acid and lipid metabolism. Indeed, solid food introduction altered the absorptive cell expression of transporters of amino acids whose concentration was reduced in the lumen. Increased utilization of milk-derived amino acids by the microbiota for bacterial growth could lower their availability (Portune et al. 2016), which could explain the lower urea concentration in the plasma and the increased expression of its

transporter (*SLC14A2*) in absorptive cells after the introduction of solid food. The effects of solid food ingestion on the expression of lipid handling genes in absorptive cells could also be driven by changes in the gut microbiota, which has previously been shown to regulate lipid homeostasis in the intestinal epithelium during the weaning transition in mice (Rakoff-Nahoum et al. 2015). Indeed, metabolites produced by the gut microbiota in early life regulate lipid metabolism in epithelial cells (Araújo et al. 2020; Shelton et al. 2023). In contrast, changes in dietary lipid supply can be ruled out, as lipids are mainly derived from maternal milk (Gidenne and Fortun-Lamothe 2002), the amount of which was not reduced after the introduction of solid food. Changes in the gut microbiota triggered by solid food ingestion could also contribute to the upregulation of basolateral bile acid exporters (OSTα/β coded by *SCL51A/B* genes) in absorptive cells and to the slight reduction of the plasmatic concentration of cholesterol, the precursor of bile acids (Rakoff-Nahoum et al. 2015; Le Roy et al. 2019; Collins et al. 2023). In turn, solid food-induced modification of bile acid metabolism could contribute to the maturation of the microbiota, as demonstrated in mice at the suckling-to-weaning transition (van Best et al. 2020). Interestingly, we found that the cytosolic bile acid binding protein (*FABP6*) was specifically expressed and upregulated in BEST4^{+} cells after solid food ingestion, which suggests an uncovered role for these cells in the enterohepatic circulation (Dawson and Karpen 2015).

Our study is focused on epithelial cells, whereas major changes are known to occur in intestinal immune cells during the weaning transition (Al Nabhani et al. 2019). Our initial scRNA-seq dataset included some intraepithelial lymphocytes but their numbers were insufficient to perform reliable analyses. Future studies analyzing the single-cell transcriptome of *lamina propria* immune cells in our suckling rabbit model ingesting or not solid food are needed to expand our understanding of the gut barrier maturation during the weaning transition. Indeed, the transcriptome changes that we observed in intestinal epithelial cells after solid food ingestion suggest alterations in the crosstalk with immune cells, particularly in relation to interferon and cytokine signaling. Another limitation of our study is related to its restriction to epithelial cells isolated from the cecum, which we chose because this gut region harbors a dense microbial

population that is highly responsive to dietary changes at the suckling-to-weaning transition (Beaumont et al. 2020). Additional studies examining single-cell transcriptome changes induced by solid food ingestion in other regions of the gut, such as the jejunum, may also be relevant to explore metabolic and immune modulations. Furthermore, previous studies have shown that microbiota changes are directly involved in epithelial bulk transcriptome modifications at the weaning transition (Rakoff-Nahoum et al. 2015; Pan et al. 2018), while our study performed at the single-cell level did not evaluate this causal role. The recent development of intestinal organoids that recapitulate the cellular diversity of the epithelium *in vitro*, including in rabbits (Mussard et al. 2020), will be useful in future studies aiming at evaluating the cell type specific transcriptome changes induced by gut bacteria or metabolites modified at the weaning transition.

Conclusion

In conclusion, our study provides the first single-cell transcriptomic atlas of the rabbit intestinal epithelium and significantly expands the understanding of cellular diversity in the mammalian intestine. We highlighted the homology between rabbit and human intestinal epithelial cells, such as BEST4^{+} cells, supporting the suitability of the rabbit as a model for gastrointestinal research. In addition, we uncovered cell type specific transcriptome modifications driven by solid food ingestion at the suckling-to-weaning transition, highlighting changes in epithelial defense mechanisms and metabolic processes. These findings contribute to a broader understanding of the postnatal maturation of the gut barrier in mammals.

Acknowledgments

This work was supported by a grant from the French National Research Agency: ANR-JCJC MetaboWean (ANR-21-CE20-0048). Tania Malonga was supported by grants from Toulouse-INP, INRAE and Oak Ridge Institute for Science and Education (ORISE). The authors thank Isabelle Fourquaux (CMEAB, Toulouse, France) for assistance with electron microscopy analyses. We acknowledge the I2MC cytometry and cell sorting facility (Genotoul-TRI), member of the national infrastructure France-BioImaging supported by the French National Research Agency (ANR-10-INBS-04).

Disclosures

The authors declare no conflict of interest.

Author contributions

CK, CLL, NV and MB designed research;

TM, CK, EL, AP, EJ, CL, MD, IP, ER, AI and MB conducted research;

TM, CC, NV and MB analyzed data;

TM, NV and MB wrote the initial draft.

All authors have read and approved the final manuscript.

FIGURE LEGENDS

Figure 1. A single-cell transcriptomic atlas of the rabbit caecum epithelium

(A) Uniform Manifold Approximation and Projection (UMAP) of cells colored by epithelial cell type. The 13,805 cells were derived from n=8 suckling rabbits ingesting or not solid food (n=4/group).

(B) Expression of selected marker genes for each cell type (average expression across cells in color and percentage of cells expressing the marker in size).

(C) UMAPs colored by the expression of marker genes of each cell type.

(D) UMAP colored by the pseudotime of the stem and absorptive cells.

(E) UMAP colored by the inferred cell cycle state.

(F) Localization of transit amplifying cells in the rabbit caecum epithelium by immunostaining of KI67 (brown). Nuclei are stained in blue. Scale bar 50 µm.

(G) Localization of BEST4^{+} cells in the rabbit caecum epithelium *by in situ* hybridization of BEST4 mRNA (red). Nuclei are stained in blue. Scale bar 50 µm.

(H) Localization of goblet cells in the rabbit caecum epithelium *by in situ* hybridization of SPINK4 mRNA (red). Nuclei are stained in blue. Scale bar 50 µm.

(I) Ultrastructural appearance of rabbit caecum epithelial cells. i) Transmission electron microscopy (TEM) observation of absorptive cells. The white arrowhead shows an electron dense absorptive cell. Scale bar 10 µm. ii) Scanning electron microscopy (SEM) observation of microvilli. White arrowheads show cells with low density of microvilli. Scale bar 5 µm. iii) v) TEM observation of a goblet cell. The white arrowhead shows mucin granules. Scale bar 5 µm. iv) SEM observation of a goblet cell. Scale bar 2 µm. v) TEM observation of an enteroendocrine cell containing basal electron dense granules (white arrowhead). Scale bar 10 µm. vi) TEM observation of Paneth-like cells containing apical electron dense granules (white arrowheads) at the crypt base. Scale bar 5 µm

AC: absorptive cells, EEC: enteroendocrine cells, TA: transit amplifying cells

Figure 2. Transcriptionally distinct cell populations in the rabbit caecum epithelium.

(A) Average expression of the top 10 marker genes with the highest average log2(fold change) for each cell type. For a given cell type, markers were ordered by decreasing log2(fold change) of the expression between this cell type and the other types.

(B) Crypt axis score for each cell type.

(C) Relative abundance for each cell type.

(D) Selected biological processes enriched in marker genes for each cell type. The color corresponds to the -log10(adjusted p-value) value of the over-representation test and the size corresponds to the percentage of marker genes among the genes of the ontology term.

AC: absorptive cells, EEC: enteroendocrine cells, TA: transit amplifying cells

Figure 3. Ingestion of solid food by suckling rabbits modulates the transcriptome of each epithelial cell type

(A) Uniform Manifold Approximation and Projection (UMAP) of epithelial cells colored by group. The left panel shows UMAP of merged datasets, with cells restricted to Milk (n=4) and Milk+Solid (n=4) groups shown independently on the middle and right panels, respectively.

(B) Number of differentially expressed genes (DEGs) between groups per cell type. Gray bars represent downregulated genes in the “Milk+Solid” group while white bars represent upregulated genes in the “Milk+Solid” group. DEG were obtained by using Negative Binomial generalized linear models on pseudo-bulk data fitted independently in each cell type.

(C) Relative abundance of each epithelial cell type. Points represent individual values in rabbits and dotted lines link littermates.

(D) Volcano plots of test results for each cell type. The -log10(adjusted p-value) values are plotted on the y-axis and the log2(fold change) values are plotted on the x-axis.

AC: absorptive cells, EEC: enteroendocrine cells, TA: transit amplifying cells

Figure 4. The transcriptomic changes induced by the introduction of solid food are predominantly cell-type specific.

(A) Number of differentially expressed genes (DEGs) that are cell type-specific or shared by multiple cell types for stem cells, mature absorptive cells, BEST4^{+} cells, and goblet cells.

(B) Selected DEGs significance (log10(adjusted p-value), color) and fold change sign (red for over expressed and blue for under expressed in the "Milk+Solid" group versus the "Milk" group) by cell type. The size represents the percentage of cells expressing the gene in the corresponding cell type.

(C-E) Expression level of selected DEGs shared between several cell types, by cell (dot) per cell type and group.

(F) Localization of PIGR mRNA (red) by *in situ* hybridization in the rabbit caecum epithelium. Nuclei are stained in blue. Scale bar 50 µm.

(G) Immunostaining of immunoglobulin A (IgA, brown) in the rabbit caecum epithelium. Nuclei are stained in blue. Scale bar 50 µm.

(H-J) Expression level of selected DEGs specific of one cell type, by cell (dot) per cell type and group.

(K) Selected biological processes enriched in DEGs of each cell type. The color corresponds to the -log10(adjusted p-value) values and the size represents the percentage of DEGs included in the biological process.

AC: absorptive cells, EEC: enteroendocrine cells, TA: transit amplifying cells

Figure 5. The introduction of solid food modifies the expression of genes involved in epithelial defenses.

(A-D) Top: Selected differentially expressed genes (DEG) significance (log10(adjusted p-value) values, color) and fold change sign (red for over expressed and blue for under expressed genes in the "Milk+Solid" group versus the "Milk" group) involved in (A) detoxification and redox balance, (B) interferon signaling, (C) cytokine signaling, (D) antimicrobial peptides. The size corresponds to the

percentage of cells expressing the gene in the cell type. Bottom: Expression level of a selected DEG by cell (dot), per cell type and group.

(E) Concentration of calprotectin in caecum epithelial cells. Points represent individual values per rabbit and dotted lines link littermates. ***: p-value < 0.001.

AC: absorptive cells, EEC: enteroendocrine cells, TA: transit amplifying cells

Figure 6. The introduction of solid food modifies the expression of genes involved in the mucus barrier, epithelial differentiation and renewal.

(A-B) Top: Selected differentially expressed genes (DEG) significance (log10(adjusted p-value) values, color) and fold change sign (red for over expressed and blue for under expressed genes in the "Milk+Solid" group versus the "Milk" group) involved in (A) glycosylation, and (B) mucus components. The size corresponds to the percentage of cells expressing the gene in the cell type. Bottom: Expression level of a selected DEG by cell (dot), per cell type and group.

(C) Representative histological observation of the caecum mucosa in each group. Alcian blue shows acidic mucins. Tissues are counterstained with hematoxylin and eosin. Scale bar 20 µm.

(D) Number of goblet cells per crypt. Points represent individual values in rabbits and dotted lines link littermates.

(E-F) Top: Selected DEG significance (log10(adjusted p-value) values, color) and fold change sign (red for over expressed and blue for under expressed genes in the "Milk+Solid" group versus the "Milk" group) involved in (E) differentiation, and (F) stemness and proliferation. The size corresponds to the percentage of cells expressing the gene in the cell type. Bottom: Expression level of a selected DEG by cell (dot), per cell type and group.

(G) Epithelial crypt depth. Points represent individual values in rabbits and dotted lines link littermates.

AC: absorptive cells, EEC: enteroendocrine cells, TA: transit amplifying cells

Figure 7. Solid food-induced modifications of the expression of genes involved in epithelial nutrient handling is associated with changes in concentrations of caecal and plasma metabolites.

(A-C) Top: Selected differentially expressed genes (DEG) significance (log10(adjusted p-value) values, color) and fold change sign (red for over expressed and blue for under expressed genes in the "Milk+Solid" group versus the "Milk" group) involved in (A) lipid metabolism, (B) epithelial transport and (C) hormone secretion. The size corresponds to the percentage of cells expressing the gene in the cell type. Bottom: Expression level of a selected DEG by cell (dot), per cell type and group.

(D) Plasmatic concentrations of metabolites. Points represent individual values per rabbit and dotted lines link littermates. *: p-value < 0.05, **: p-value < 0.01, ***: p-value < 0.001. HDL: high-density lipoprotein; LDL: low-density lipoprotein.

(E) Relative caecal concentrations of metabolites detected by nuclear magnetic resonance-based metabolomics. Points represent individual values per rabbit and dotted lines link littermates. *: adjusted p-value <0.05, **: adjusted p-value <0.01, ***: adjusted p-value <0.001.

AC: absorptive cells, EEC: enteroendocrine cells, TA: transit amplifying cells

SUPPLEMENTAL FIGURE LEGENDS

Figure S1. Experimental design.

(A) Schematic representation of the experimental design repeated for n=4 litters. From day (D) 0 to D4, the pups (n=10) were housed in the same cage as their dam. From D4 to D12, the pups were placed in a separate cage and were moved to the nest of the dam's cage once a day for 5-10 minutes of suckling. At D12, the litter size was reduced to 6 in order to maximize milk availability. From D12 to D24/25, the same procedure was used for suckling and half of the pups were moved to a cage with access to solid food pellets. On D24/25, littermate pups from each group (n=1 pup/litter/group) were sacrificed for the isolation of cecal epithelial cells and single-cell RNA-sequencing.

(B) Rabbit weights at D12 and D24/25.

(C) Total milk intake per rabbit between D12 and D24/25.

(D) Total solid feed intake per rabbit between D12 and D24/25.

(E) Full caecum weight per rabbit. ***: p-value < 0.001.

(B-E): Points represent individual values in rabbits and dotted lines link littermates.

Figure S2. Quality controls of single-cell transcriptomics.

(A) Counts, number of expressed genes, and percentage of mitochondrial gene reads per cell and rabbit before filtering.

(B) Counts, number of expressed genes, and percentage of mitochondrial gene reads per cell and rabbit after filtering.

(C) Uniform Manifold Approximation and Projection (UMAP) of cells colored by the total counts per cell.

(D) UMAP colored by the number of expressed genes.

(E) UMAP colored by the percentage of mitochondrial gene reads.

(F) UMAP colored by the clusters identified with the *FindClusters* function of Seurat.

(G) Expression of the top 50 genes with the highest average log2(fold change) of each cluster. For a given cluster, markers were ordered by decreasing log2(fold-change) of the expression between this cluster and the other clusters. Cell clusters are indicated by numbers and colored bars on the top.

Figure S3. Cell type annotation.

(A) Pseudo-time distribution of absorptive cells (AC). The area under the curve is colored with respect to chosen AC subset borders.

(B) Pseudo-time distribution in stem cells and AC subsets.

(C) Uniform Manifold Approximation and Projection (UMAP) colored by label transfer from adult and fetal human large intestine epithelial cells to rabbit caecal epithelial cells.

(D) UMAP colored by mapping score calculated using the large intestine human intestinal epithelium.

(E) UMAP colored by epithelial cell types for each rabbit order by groups (rows) and litters (columns).

AC: absorptive cells, EC: enterochromaffin cells, EEC: enteroendocrine cells, TA: transit amplifying cells.

Figure S4. Principal component analysis of pseudo-bulk data.

Principal components analysis (PCA) performed on pseudo-bulk data for each epithelial cell type. Individual samples are represented by the rabbit (R) identifier. The dotted lines connect rabbit littermates. AC: absorptive cells, EEC: enteroendocrine cells, TA: transit amplifying cells.

SUPPLEMENTAL TABLE LEGENDS

Table S1. Marker genes of each cell type

List of the marker genes of each cell type (presented in separate tabs) identified by using the *FindAllMarkers* function of Seurat. Columns give the gene name, the *p*-value of the Wilcoxon rank test, the adjusted p-value (Bonferroni procedure), and the average log2 fold-change. Pct.1 is the percentage of cells expressing the gene in the cell type indicated in the tab name, while pct.2 is the percentage of cells expressing the gene in all other cell types. AC: absorptive cells, EEC: enteroendocrine cells, TA: transit amplifying cells.

Table S2. Biological pathways enriched in the marker genes of each cell type

List of biological pathways enriched in the marker genes of each cell type (presented in separate tabs). Columns give the Gene Ontology (GO) identifier (ID), the pathway name (Description), the GeneRatio (number of marker genes over the number of genes in the biological pathway), the BgRatio (total number of genes in the biological pathway over the total number of genes expressed in the scRNA-seq dataset), the p-value and the adjusted p-value (Benjamini-Hochberg procedure) of the over-representation test, and the geneID (list of marker genes in the biological pathway), respectively. AC: absorptive cells, EEC: enteroendocrine cells, TA: transit amplifying cells.

Table S3. Differentially expressed genes between groups in each cell type

List of the differentially expressed genes (DEGs) between groups ("Milk" vs "Milk+Solid") in each cell type (presented in separate tabs) identified by fitting Negative Binomial generalized linear models on pseudo-bulk data in each cell type independently. The columns give the gene name, the log2(fold change), the log counts per million (CPM) reads, the likelihood (LR) ratio, the p-value (LR test), the adjusted p-value (Benjamini-Hochberg procedure), and the over or under-expressed state of the gene in the "Milk + Solid" group versus the "Milk" group, respectively. AC: absorptive cells, EEC: enteroendocrine cells, TA: transit amplifying cells.

Table S4. Biological pathways enriched in differentially expressed genes between groups in each cell type.

List of biological pathways enriched in differentially expressed genes (DEGs) between groups ("Milk" vs "Milk+Solid") per cell type. Columns give the Gene Ontology (GO) identifier (ID), the pathway name (Description), the GeneRatio (number of DEG over the number of genes in the biological pathway), the BgRatio (total number of genes in the biological pathway over the total number of genes expressed in the scRNA-seq dataset), the p-value and the adjusted p-value (Benjamini-Hochberg procedure) of the over-representation test, and the geneID (list of DEGs in the biological pathway). AC: absorptive cells, EEC: enteroendocrine cells, TA: transit amplifying cells.

Table S5. Bacterial relative abundance in the caecum.

Relative abundances of bacterial taxa at the phylum, family, and genus level in the caecum content of rabbits determined by 16S rRNA gene amplicon sequencing. Columns give the *p*-value (linear mixed model), the adjusted *p*-value, the mean relative abundance per group, and the standard error of the mean (SEM) for each taxa which abundance was > 0.5% in at least one group (repeatability threshold for quantitative analyses).

REFERENCES

Al Nabhani Z, Dulauroy S, Marques R, et al (2019) A Weaning Reaction to Microbiota Is Required for Resistance to Immunopathologies in the Adult. Immunity 50:1276-1288.e5. https://doi.org/10.1016/j.immuni.2019.02.014

Araújo JR, Tazi A, Burlen-Defranoux O, et al (2020) Fermentation Products of Commensal Bacteria Alter Enterocyte Lipid Metabolism. Cell Host & Microbe 27:358-375.e7. https://doi.org/10.1016/j.chom.2020.01.028

Arike L, Holmén-Larsson J, Hansson GC (2017) Intestinal Muc2 mucin O-glycosylation is affected by microbiota and regulated by differential expression of glycosyltranferases. Glycobiology 27:318–328. https://doi.org/10.1093/glycob/cww134

Bang Y-J (2023) Vitamin A: a key coordinator of host-microbe interactions in the intestine. BMB Reports 56:133–139. https://doi.org/10.5483/BMBRep.2023-0005

Barker N (2014) Adult intestinal stem cells: critical drivers of epithelial homeostasis and regeneration. Nat Rev Mol Cell Biol 15:19–33. https://doi.org/10.1038/nrm3721

Bar-Shira E, Cohen I, Elad O, Friedman A (2014) Role of goblet cells and mucin layer in protecting maternal IgA in precocious birds. Developmental & Comparative Immunology 44:186–194. https://doi.org/10.1016/j.dci.2013.12.010

Beaumont M, Mussard E, Barilly C, et al (2022) Developmental Stage, Solid Food Introduction, and Suckling Cessation Differentially Influence the Comaturation of the Gut Microbiota and Intestinal Epithelium in Rabbits. The Journal of Nutrition 152:723–736. https://doi.org/10.1093/jn/nxab411

Beaumont M, Païs C, Mussard E, et al (2020) Gut microbiota derived metabolites contribute to intestinal barrier maturation at the suckling-to-weaning transition. Gut Microbes 11:1268–1286. https://doi.org/10.1080/19490976.2020.1747335

Benjamini Y, Hochberg Y (1995) Controlling the False Discovery Rate: A Practical and Powerful Approach to Multiple Testing. Journal of the Royal Statistical Society Series B: Statistical Methodology 57:289–300. https://doi.org/10.1111/j.2517-6161.1995.tb02031.x

Beumer J, Puschhof J, Bauzá-Martinez J, et al (2020) High-Resolution mRNA and Secretome Atlas of Human Enteroendocrine Cells. Cell 181:1291-1306.e19. https://doi.org/10.1016/j.cell.2020.04.036

Beumer J, Puschhof J, Yengej FY, et al (2022) BMP gradient along the intestinal villus axis controls zonated enterocyte and goblet cell states. Cell Reports 38:110438. https://doi.org/10.1016/j.celrep.2022.110438

Biol-N'garagba M-C, Louisot P (2003) Regulation of the intestinal glycoprotein glycosylation during postnatal development: role of hormonal and nutritional factors. Biochimie 85:331–352. https://doi.org/10.1016/S0300-9084(03)00039-7

Burclaff J, Bliton RJ, Breau KA, et al (2022) A Proximal-to-Distal Survey of Healthy Adult Human Small Intestine and Colon Epithelium by Single-Cell Transcriptomics. Cellular and Molecular Gastroenterology and Hepatology 13:1554–1589. https://doi.org/10.1016/j.jcmgh.2022.02.007

Butler A, Hoffman P, Smibert P, et al (2018) Integrating single-cell transcriptomic data across different conditions, technologies, and species. Nat Biotechnol 36:411–420. https://doi.org/10.1038/nbt.4096

Collins SL, Stine JG, Bisanz JE, et al (2023) Bile acids and the gut microbiota: metabolic interactions and impacts on disease. Nat Rev Microbiol 21:236–247. https://doi.org/10.1038/s41579-022-00805-x

Cui C, Li L, Wu L, et al (2023) Paneth cells in farm animals: current status and future direction. J Anim Sci Biotechnol 14:118. https://doi.org/10.1186/s40104-023-00905-5

Dawson PA, Karpen SJ (2015) Intestinal transport and metabolism of bile acids. Journal of Lipid Research 56:1085–1099. https://doi.org/10.1194/jlr.R054114

Díez-Sánchez A, Lindholm HT, Vornewald PM, et al (2024) LSD1 drives intestinal epithelial maturation and controls small intestinal immune cell composition independent of microbiota in a murine model. Nat Commun 15:3412. https://doi.org/10.1038/s41467-024-47815-2

Elmentaite R, Kumasaka N, Roberts K, et al (2021) Cells of the human intestinal tract mapped across space and time. Nature 597:250–255. https://doi.org/10.1038/s41586-021-03852-1

Elmentaite R, Ross ADB, Roberts K, et al (2020) Single-Cell Sequencing of Developing Human Gut Reveals Transcriptional Links to Childhood Crohn's Disease. Developmental Cell 55:771-783.e5. https://doi.org/10.1016/j.devcel.2020.11.010

Escudié F, Auer L, Bernard M, et al (2018) FROGS: Find, Rapidly, OTUs with Galaxy Solution. Bioinformatics 34:1287–1294. https://doi.org/10.1093/bioinformatics/btx791

Fawkner-Corbett D, Antanaviciute A, Parikh K, et al (2021) Spatiotemporal analysis of human intestinal development at single-cell resolution. Cell 184:810-826.e23. https://doi.org/10.1016/j.cell.2020.12.016

Frazer LC, Good M (2022) Intestinal epithelium in early life. Mucosal Immunol 15:1181–1187. https://doi.org/10.1038/s41385-022-00579-8

Gidenne T, Fortun-Lamothe L (2002) Feeding strategy for young rabbits around weaning: a review of digestive capacity and nutritional needs. Animal Science 75:169–184. https://doi.org/10.1017/S1357729800052942

Gidenne T, Lebas F (2006) Feeding behaviour in rabbits. In: Bels V (ed) Feeding in domestic vertebrates: from structure to behaviour, 1st edn. CABI, UK, pp 179–194

Hall JA, Grainger JR, Spencer SP, Belkaid Y (2011) The Role of Retinoic Acid in Tolerance and Immunity. Immunity 35:13–22. https://doi.org/10.1016/j.immuni.2011.07.002

Hansson J, Panchaud A, Favre L, et al (2011) Time-resolved Quantitative Proteome Analysis of *In Vivo* Intestinal Development. Molecular & Cellular Proteomics 10:M110.005231. https://doi.org/10.1074/mcp.M110.005231

Henning SJ (1981) Postnatal development: coordination of feeding, digestion, and metabolism. Am J Physiol 241:G199-214. https://doi.org/10.1152/ajpgi.1981.241.3.G199

Holmes JL, Van Itallie CM, Rasmussen JE, Anderson JM (2006) Claudin profiling in the mouse during postnatal intestinal development and along the gastrointestinal tract reveals complex expression patterns. Gene Expr Patterns 6:581–588. https://doi.org/10.1016/j.modgep.2005.12.001

Hornef MW, Torow N (2020) 'Layered immunity' and the 'neonatal window of opportunity' – timed succession of non-redundant phases to establish mucosal host–microbial homeostasis after birth. Immunology 159:15–25. https://doi.org/10.1111/imm.13149

Ilchmann-Diounou H, Menard S (2020) Psychological Stress, Intestinal Barrier Dysfunctions, and Autoimmune Disorders: An Overview. Front Immunol 11:. https://doi.org/10.3389/fimmu.2020.01823

Jenkins SL, Wang J, Vazir M, et al (2003) Role of passive and adaptive immunity in influencing enterocyte-specific gene expression. American Journal of Physiology-Gastrointestinal and Liver Physiology 285:G714–G725. https://doi.org/10.1152/ajpgi.00130.2003

Knoop KA, Newberry RD (2018) Goblet cells: multifaceted players in immunity at mucosal surfaces. Mucosal Immunology 11:1551–1557. https://doi.org/10.1038/s41385-018-0039-y

Layunta E, Jäverfelt S, Dolan B, et al (2021) IL-22 promotes the formation of a MUC17 glycocalyx barrier in the postnatal small intestine during weaning. Cell Reports 34:108757. https://doi.org/10.1016/j.celrep.2021.108757

Le Roy T, Lécuyer E, Chassaing B, et al (2019) The intestinal microbiota regulates host cholesterol homeostasis. BMC Biology 17:94. https://doi.org/10.1186/s12915-019-0715-8

Malonga T, Vialaneix N, Beaumont M (2024) BEST4+ cells in the intestinal epithelium. American Journal of Physiology-Cell Physiology. https://doi.org/10.1152/ajpcell.00042.2024

Ménard S, Förster V, Lotz M, et al (2008) Developmental switch of intestinal antimicrobial peptide expression. J Exp Med 205:183–193. https://doi.org/10.1084/jem.20071022

Moor AE, Harnik Y, Ben-Moshe S, et al (2018) Spatial Reconstruction of Single Enterocytes Uncovers Broad Zonation along the Intestinal Villus Axis. Cell 175:1156-1167.e15. https://doi.org/10.1016/j.cell.2018.08.063

Muncan V, Heijmans J, Krasinski SD, et al (2011) Blimp1 regulates the transition of neonatal to adult intestinal epithelium. Nat Commun 2:452. https://doi.org/10.1038/ncomms1463

Murphy AE, Skene NG (2022) A balanced measure shows superior performance of pseudobulk methods in single-cell RNA-sequencing analysis. Nat Commun 13:7851. https://doi.org/10.1038/s41467-022-35519-4

Mussard E, Pouzet C, Helies V, et al (2020) Culture of rabbit caecum organoids by reconstituting the intestinal stem cell niche *in vitro* with pharmacological inhibitors or L-WRN conditioned medium. Stem Cell Research 48:101980. https://doi.org/10.1016/j.scr.2020.101980

Nanthakumar NN, Henning SJ (1993) Ontogeny of sucrase-isomaltase gene expression in rat intestine: responsiveness to glucocorticoids. Am J Physiol 264:G306-311. https://doi.org/10.1152/ajpgi.1993.264.2.G306

Nanthakumar NN, Meng D, Newburg DS (2013) Glucocorticoids and microbiota regulate ontogeny of intestinal fucosyltransferase 2 requisite for gut homeostasis. Glycobiology 23:1131–1141. https://doi.org/10.1093/glycob/cwt050

Navis M, Martins Garcia T, Renes IB, et al (2019) Mouse fetal intestinal organoids: new model to study epithelial maturation from suckling to weaning. EMBO Rep 20:e46221. https://doi.org/10.15252/embr.201846221

Paës C, Gidenne T, Bébin K, et al (2020) Early Introduction of Solid Feeds: Ingestion Level Matters More Than Prebiotic Supplementation for Shaping Gut Microbiota. Frontiers in Veterinary Science 7:

Palmer MV, Wiarda J, Kanipe C, Thacker TC (2019) Early Pulmonary Lesions in Cattle Infected via Aerosolized Mycobacterium bovis. Vet Pathol 56:544–554. https://doi.org/10.1177/0300985819833454

Pan W-H, Sommer F, Falk-Paulsen M, et al (2018) Exposure to the gut microbiota drives distinct methylome and transcriptome changes in intestinal epithelial cells during postnatal development. Genome Med 10:27. https://doi.org/10.1186/s13073-018-0534-5

Parikh K, Antanaviciute A, Fawkner-Corbett D, et al (2019) Colonic epithelial cell diversity in health and inflammatory bowel disease. Nature 567:49–55. https://doi.org/10.1038/s41586-019-0992-y

Peterson LW, Artis D (2014) Intestinal epithelial cells: regulators of barrier function and immune homeostasis. Nat Rev Immunol 14:141–153. https://doi.org/10.1038/nri3608

Portune KJ, Beaumont M, Davila A-M, et al (2016) Gut microbiota role in dietary protein metabolism and health-related outcomes: The two sides of the coin. Trends in Food Science & Technology 57:213–232. https://doi.org/10.1016/j.tifs.2016.08.011

Price AE, Shamardani K, Lugo KA, et al (2018) A Map of Toll-like Receptor Expression in the Intestinal Epithelium Reveals Distinct Spatial, Cell Type-Specific, and Temporal Patterns. Immunity 49:560-575.e6. https://doi.org/10.1016/j.immuni.2018.07.016

Rakoff-Nahoum S, Kong Y, Kleinstein SH, et al (2015) Analysis of gene–environment interactions in postnatal development of the mammalian intestine. Proceedings of the National Academy of Sciences 112:1929–1936. https://doi.org/10.1073/pnas.1424886112

Robinson MD, McCarthy DJ, Smyth GK (2010) edgeR: a Bioconductor package for differential expression analysis of digital gene expression data. Bioinformatics 26:139–140. https://doi.org/10.1093/bioinformatics/btp616

Schiering C, Krausgruber T, Chomka A, et al (2014) The alarmin IL-33 promotes regulatory T-cell function in the intestine. Nature 513:564–568. https://doi.org/10.1038/nature13577

Schilderink R, Verseijden C, Seppen J, et al (2016) The SCFA butyrate stimulates the epithelial production of retinoic acid via inhibition of epithelial HDAC. American Journal of Physiology-Gastrointestinal and Liver Physiology 310:G1138–G1146. https://doi.org/10.1152/ajpgi.00411.2015

Schumacher MA (2023) The emerging roles of deep crypt secretory cells in colonic physiology. American Journal of Physiology-Gastrointestinal and Liver Physiology 325:G493–G500. https://doi.org/10.1152/ajpgi.00093.2023

Shelton CD, Sing E, Mo J, et al (2023) An early-life microbiota metabolite protects against obesity by regulating intestinal lipid metabolism. Cell Host & Microbe 31:1604-1619.e10. https://doi.org/10.1016/j.chom.2023.09.002

Silverman JB, Vega PN, Tyska MJ, Lau KS (2024) Intestinal Tuft Cells: Morphology, Function, and Implications for Human Health. Annu Rev Physiol 86:479–504. https://doi.org/10.1146/annurev-physiol-042022-030310

Sommer F, Nookaew I, Sommer N, et al (2015) Site-specific programming of the host epithelial transcriptome by the gut microbiota. Genome Biology 16:62. https://doi.org/10.1186/s13059-015-0614-4

Stuart T, Butler A, Hoffman P, et al (2019) Comprehensive Integration of Single-Cell Data. Cell 177:1888-1902.e21. https://doi.org/10.1016/j.cell.2019.05.031

Tomas J, Reygner J, Mayeur C, et al (2015) Early colonizing Esche richia coli elicits remodeling of rat colonic epithelium shifting toward a new homeostatic state. ISME J 9:46–58. https://doi.org/10.1038/ismej.2014.111

Trachsel J, Briggs C, Gabler NK, et al (2019) Dietary Resistant Potato Starch Alters Intestinal Microbial Communities and Their Metabolites, and Markers of Immune Regulation and Barrier Function in Swine. Front Immunol 10:. https://doi.org/10.3389/fimmu.2019.01381

Tsang DKL, Wang RJ, De Sa O, et al (2022) A single cell survey of the microbial impacts on the mouse small intestinal epithelium. Gut Microbes 14:2108281. https://doi.org/10.1080/19490976.2022.2108281

Vacca M, Celano G, Calabrese FM, et al (2020) The Controversial Role of Human Gut Lachnospiraceae. Microorganisms 8:573. https://doi.org/10.3390/microorganisms8040573

van Best N, Rolle-Kampczyk U, Schaap FG, et al (2020) Bile acids drive the newborn's gut microbiota maturation. Nat Commun 11:3692. https://doi.org/10.1038/s41467-020-17183-8

Van Winkle JA, Peterson ST, Kennedy EA, et al (2022) Homeostatic interferon-lambda response to bacterial microbiota stimulates preemptive antiviral defense within discrete pockets of intestinal epithelium. eLife 11:e74072. https://doi.org/10.7554/eLife.74072

Wiarda JE, Becker SR, Sivasankaran SK, Loving CL (2023) Regional epithelial cell diversity in the small intestine of pigs. Journal of Animal Science 101:skac318. https://doi.org/10.1093/jas/skac318

Yu G, Wang L-G, Han Y, He Q-Y (2012) clusterProfiler: an R Package for Comparing Biological Themes Among Gene Clusters. OMICS 16:284–287. https://doi.org/10.1089/omi.2011.0118

Zimmerman KD, Espeland MA, Langefeld CD (2021) A practical solution to pseudoreplication bias in single-cell studies. Nat Commun 12:738. https://doi.org/10.1038/s41467-021-21038-1

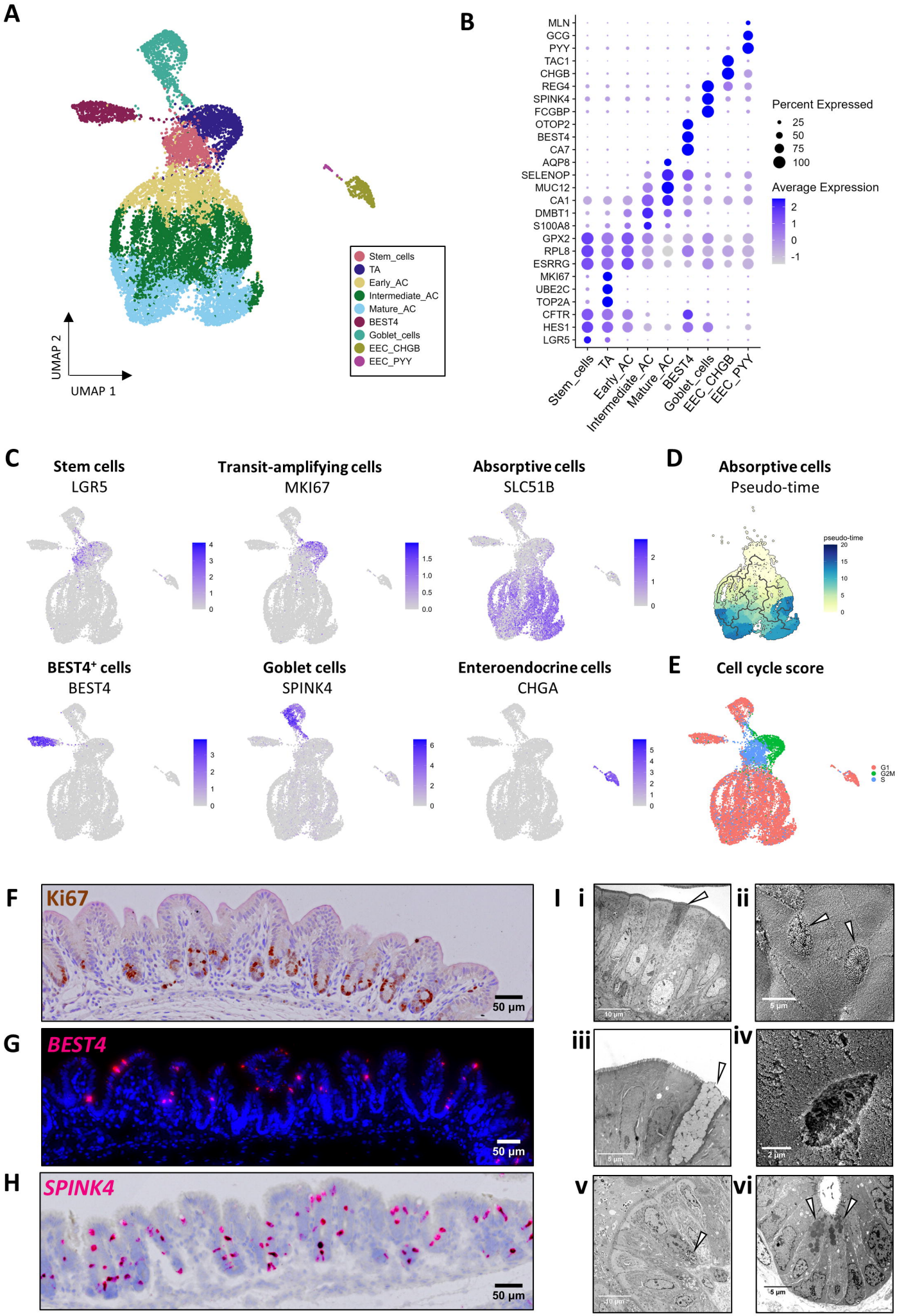
A
UMAP 2
UMAP 1
Stem_cells
TA
Early_AC
Intermediate_AC
Mature_AC
BEST4
Goblet_cells
EEC_CHGB
EEC_PYY
B
MLN
GCG
PYY
TAC1
CHGB
REG4
SPINK4
FCGBP
OTOP2
BEST4
CA7
AQP8
SELENOP
MUC12
CA1
DMBT1
S100A8
GPX2
RPL8
ESRRG
MKI67
UBE2C
TOP2A
CFTR
HES1
LGR5
Stem_cells
TA
Early_AC
Intermediate_AC
Mature_AC
BEST4
Goblet_cells
EEC_CHGB
EEC_PYY
Percent Expressed
25
50
75
100
Average Expression
2
1
0
-1
C
Stem cells
LGR5
Transit-amplifying cells
MKI67
Absorptive cells
SLC51B
BEST4⁺ cells
BEST4
Goblet cells
SPINK4
Enteroendocrine cells
CHGA
D
Absorptive cells
Pseudo-time
pseudo-time
E
Cell cycle score
G1
G2M
S
F
Ki67
50 µm
G
BEST4
50 µm
H
SPINK4
50 µm
I
i
ii
iii
iv
v
vi

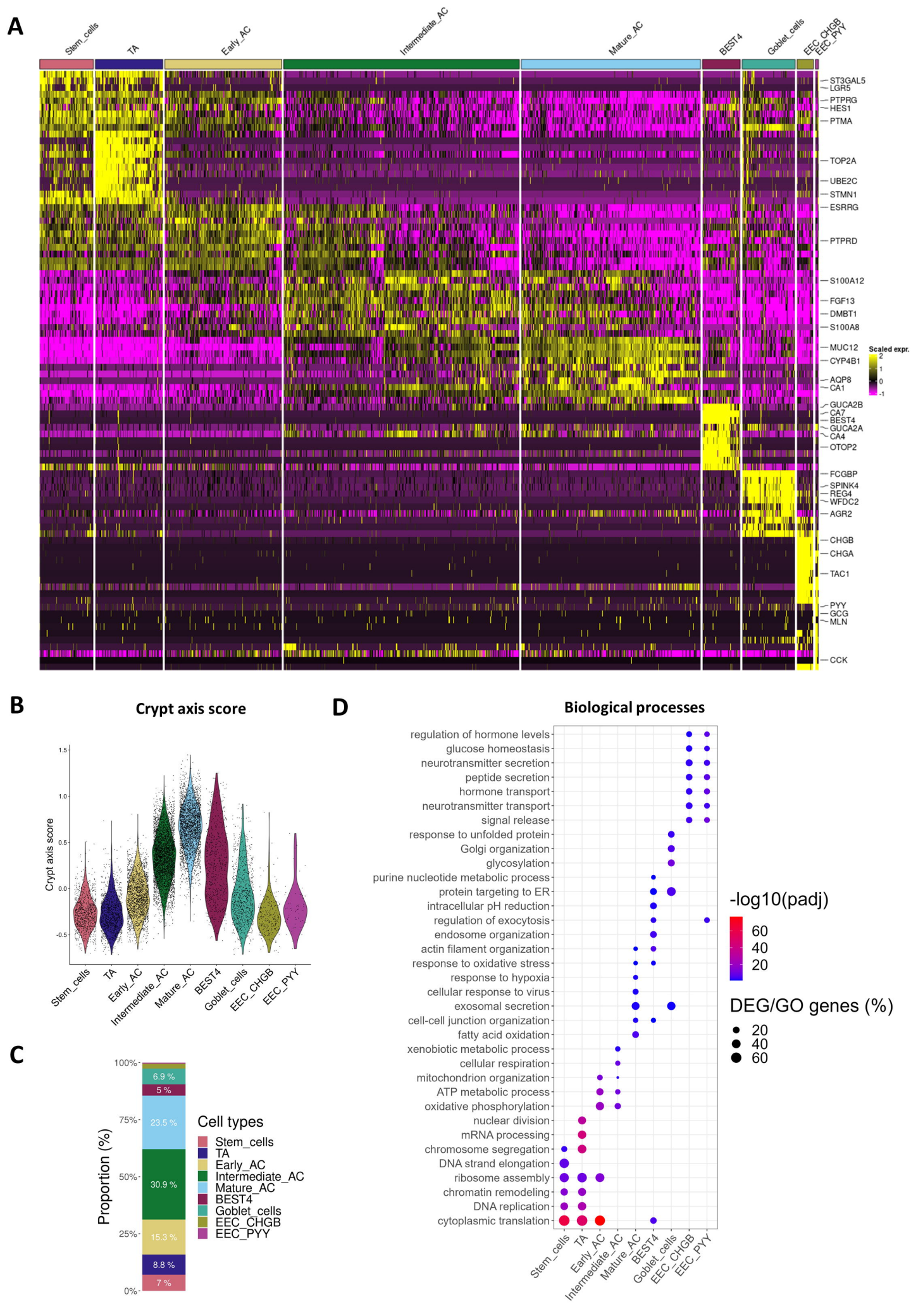
A
Stem_cells
TA
Early_AC
Intermediate_AC
Mature_AC
BEST4
Goblet_cells
EEC_CHGB
EEC_PYY
ST3GAL5
LGR5
PTPRG
HES1
PTMA
TOP2A
UBE2C
STMN1
ESRRG
PTPRD
S100A12
FGF13
DMBT1
S100A8
MUC12
CYP4B1
AQP8
CA1
GUCA2B
CA7
BEST4
GUCA2A
CA4
OTOP2
FCGBP
SPINK4
REG4
WFDC2
AGR2
CHGB
CHGA
TAC1
PYY
GCG
MLN
CCK
Scaled expr.
2
1
0
-1
B
Crypt axis score
Crypt axis score
1.5
1.0
0.5
0.0
-0.5
Stem_cells
TA
Early_AC
Intermediate_AC
Mature_AC
BEST4
Goblet_cells
EEC_CHGB
EEC_PYY
C
100%
75%
50%
25%
0%
Proportion (%)
6.9 %
5 %
23.5 %
30.9 %
15.3 %
8.8 %
7 %
Cell types
Stem_cells
TA
Early_AC
Intermediate_AC
Mature_AC
BEST4
Goblet_cells
EEC_CHGB
EEC_PYY
D
Biological processes
regulation of hormone levels
glucose homeostasis
neurotransmitter secretion
peptide secretion
hormone transport
neurotransmitter transport
signal release
response to unfolded protein
Golgi organization
glycosylation
purine nucleotide metabolic process
protein targeting to ER
intracellular pH reduction
regulation of exocytosis
endosome organization
actin filament organization
response to oxidative stress
response to hypoxia
cellular response to virus
exosomal secretion
cell-cell junction organization
fatty acid oxidation
xenobiotic metabolic process
cellular respiration
mitochondrion organization
ATP metabolic process
oxidative phosphorylation
nuclear division
mRNA processing
chromosome segregation
DNA strand elongation
ribosome assembly
chromatin remodeling
DNA replication
cytoplasmic translation
Stem_cells
TA
Early_AC
Intermediate_AC
Mature_AC
BEST4
Goblet_cells
EEC_CHGB
EEC_PYY
-log10(padj)
60
40
20
DEG/GO genes (%)
20
40
60

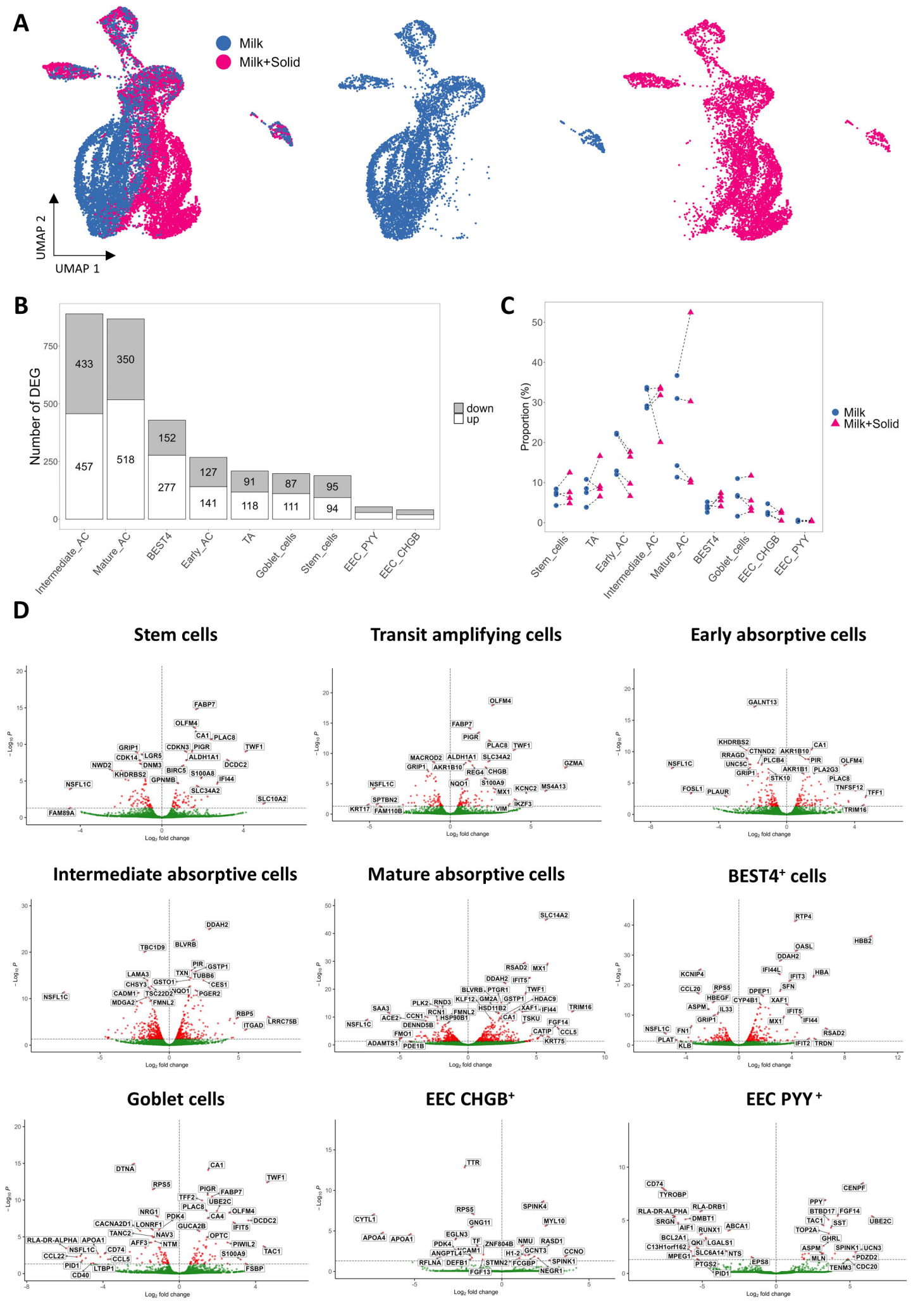
A
Milk
Milk+Solid
UMAP 2
UMAP 1
B
Number of DEG
down
up
433
350
457
518
152
277
127
141
91
118
87
111
95
94
Intermediate_AC
Mature_AC
BEST4
Early_AC
TA
Goblet_cells
Stem_cells
EEC_PYY
EEC_CHGB
C
Proportion (%)
Milk
Milk+Solid
Stem_cells
TA
Early_AC
Intermediate_AC
Mature_AC
BEST4
Goblet_cells
EEC_CHGB
EEC_PYY
D
Stem cells
Transit amplifying cells
Early absorptive cells
Intermediate absorptive cells
Mature absorptive cells
BEST4+ cells
Goblet cells
EEC CHGB+
EEC PYY+
Log2 fold change
−Log10 P

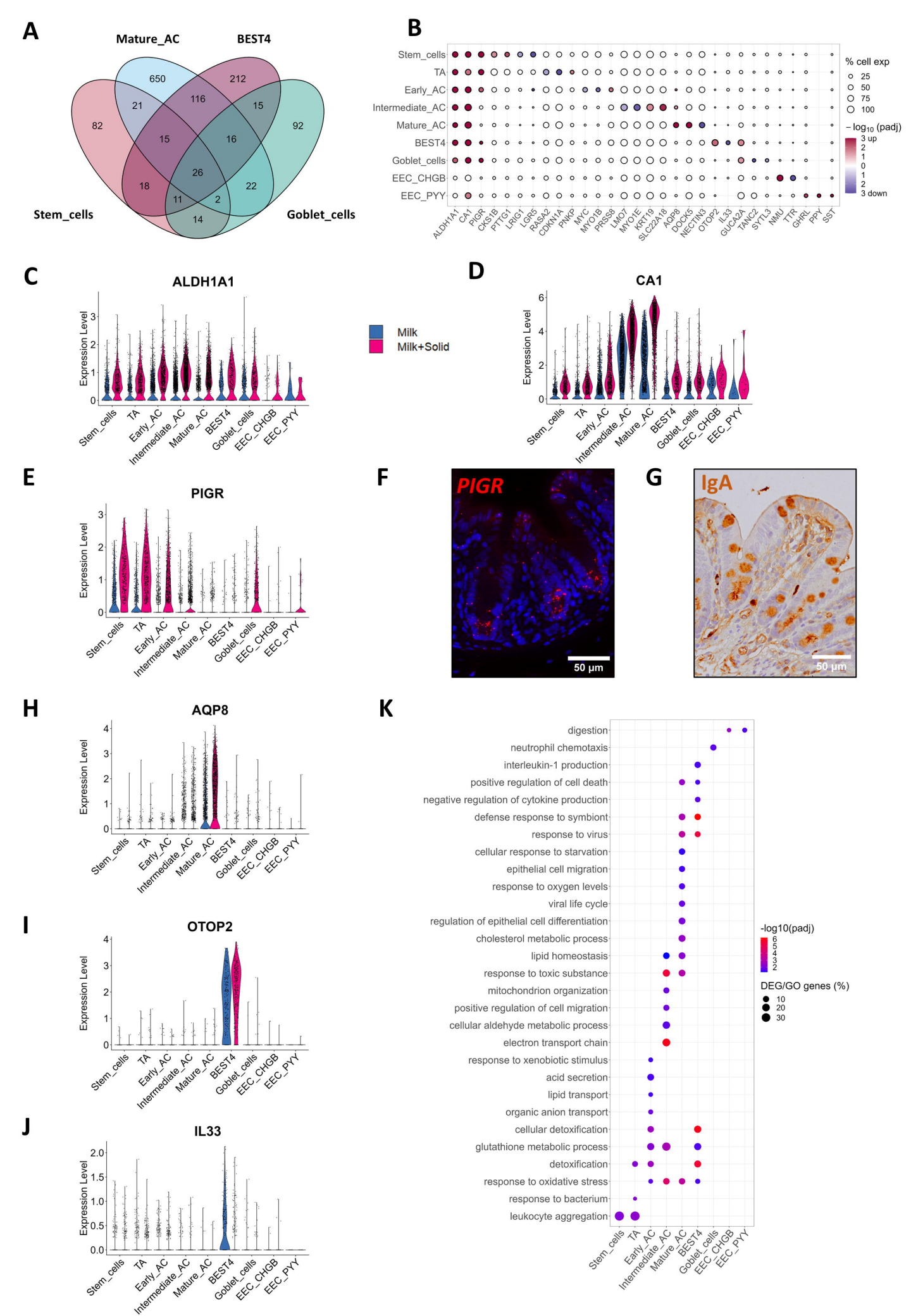
A
Mature_AC
BEST4
Stem_cells
Goblet_cells
650
212
82
92
21
116
15
15
16
26
18
22
11
2
14
B
Stem_cells
TA
Early_AC
Intermediate_AC
Mature_AC
BEST4
Goblet_cells
EEC_CHGB
EEC_PYY
ALDH1A1
CA1
PIGR
CKS1B
PTTG1
LRIG1
LGR5
RASA2
CDKN1A
PNKP
MYC
MYO1B
PRSS8
LMO7
MYO1E
KRT19
SLC22A18
AQP8
DOCK5
NECTIN3
OTOP2
IL33
GUCA2A
TANC2
SYTL3
NMU
TTR
GHRL
PPY
SST
% cell exp
25
50
75
100
– log10 (padj)
3 up
2
1
0
1
2
3 down
C
ALDH1A1
Expression Level
Milk
Milk+Solid
D
CA1
E
PIGR
F
PIGR
50 µm
G
IgA
50 µm
H
AQP8
I
OTOP2
J
IL33
K
digestion
neutrophil chemotaxis
interleukin-1 production
positive regulation of cell death
negative regulation of cytokine production
defense response to symbiont
response to virus
cellular response to starvation
epithelial cell migration
response to oxygen levels
viral life cycle
regulation of epithelial cell differentiation
cholesterol metabolic process
lipid homeostasis
response to toxic substance
mitochondrion organization
positive regulation of cell migration
cellular aldehyde metabolic process
electron transport chain
response to xenobiotic stimulus
acid secretion
lipid transport
organic anion transport
cellular detoxification
glutathione metabolic process
detoxification
response to oxidative stress
response to bacterium
leukocyte aggregation
-log10(padj)
DEG/GO genes (%)
10
20
30

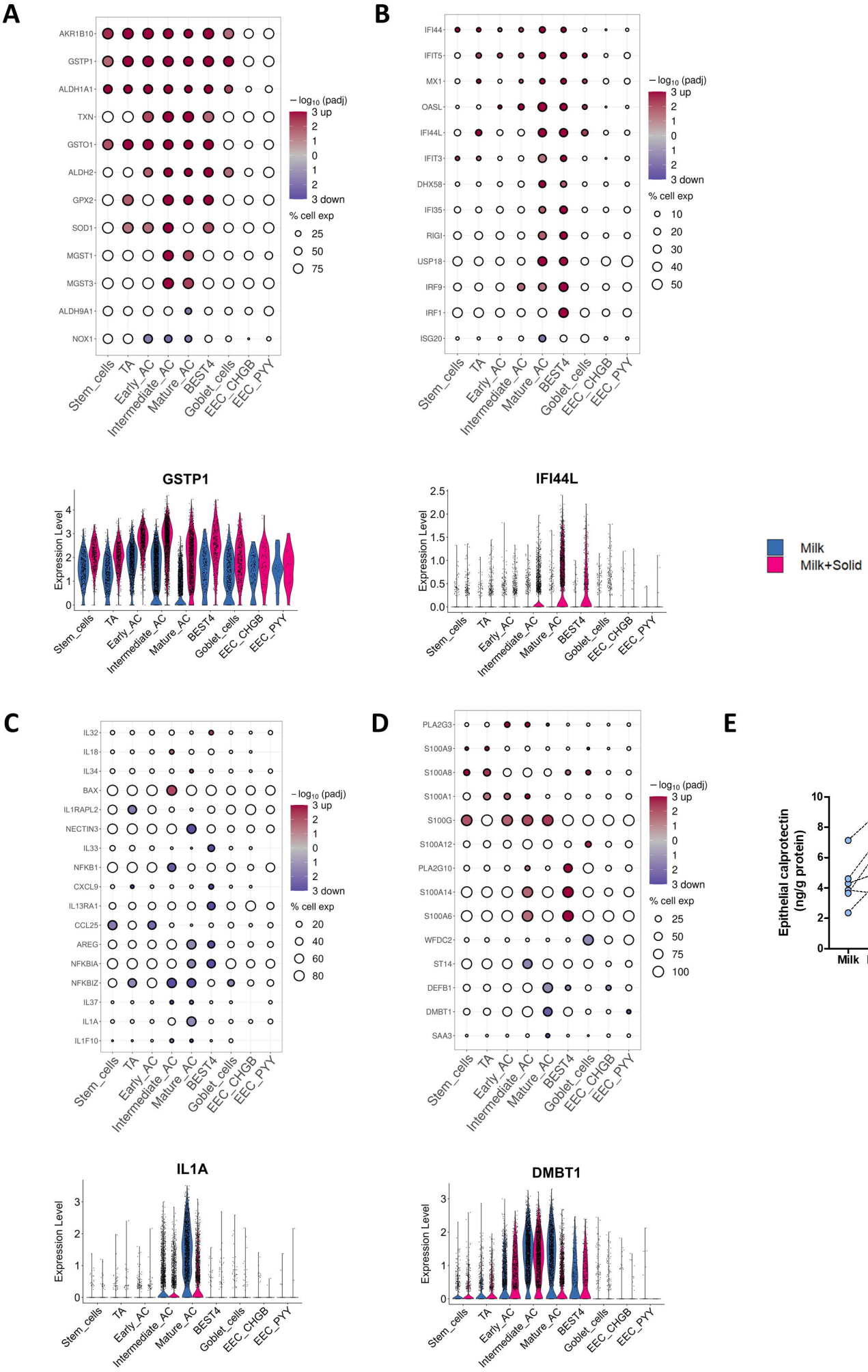
A
AKR1B10
GSTP1
ALDH1A1
TXN
GSTO1
ALDH2
GPX2
SOD1
MGST1
MGST3
ALDH9A1
NOX1
Stem_cells
TA
Early_AC
Intermediate_AC
Mature_AC
BEST4
Goblet_cells
EEC_CHGB
EEC_PYY
− log10 (padj)
3 up
2
1
0
1
2
3 down
% cell exp
25
50
75
B
IFI44
IFIT5
MX1
OASL
IFI44L
IFIT3
DHX58
IFI35
RIGI
USP18
IRF9
IRF1
ISG20
% cell exp
10
20
30
40
50
GSTP1
IFI44L
Expression Level
Milk
Milk+Solid
C
IL32
IL18
IL34
BAX
IL1RAPL2
NECTIN3
IL33
NFKB1
CXCL9
IL13RA1
CCL25
AREG
NFKBIA
NFKBIZ
IL37
IL1A
IL1F10
% cell exp
20
40
60
80
D
PLA2G3
S100A9
S100A8
S100A1
S100G
S100A12
PLA2G10
S100A14
S100A6
WFDC2
ST14
DEFB1
DMBT1
SAA3
% cell exp
25
50
75
100
E
***
Epithelial calprotectin (ng/g protein)
Milk
Milk+Solid
IL1A
DMBT1

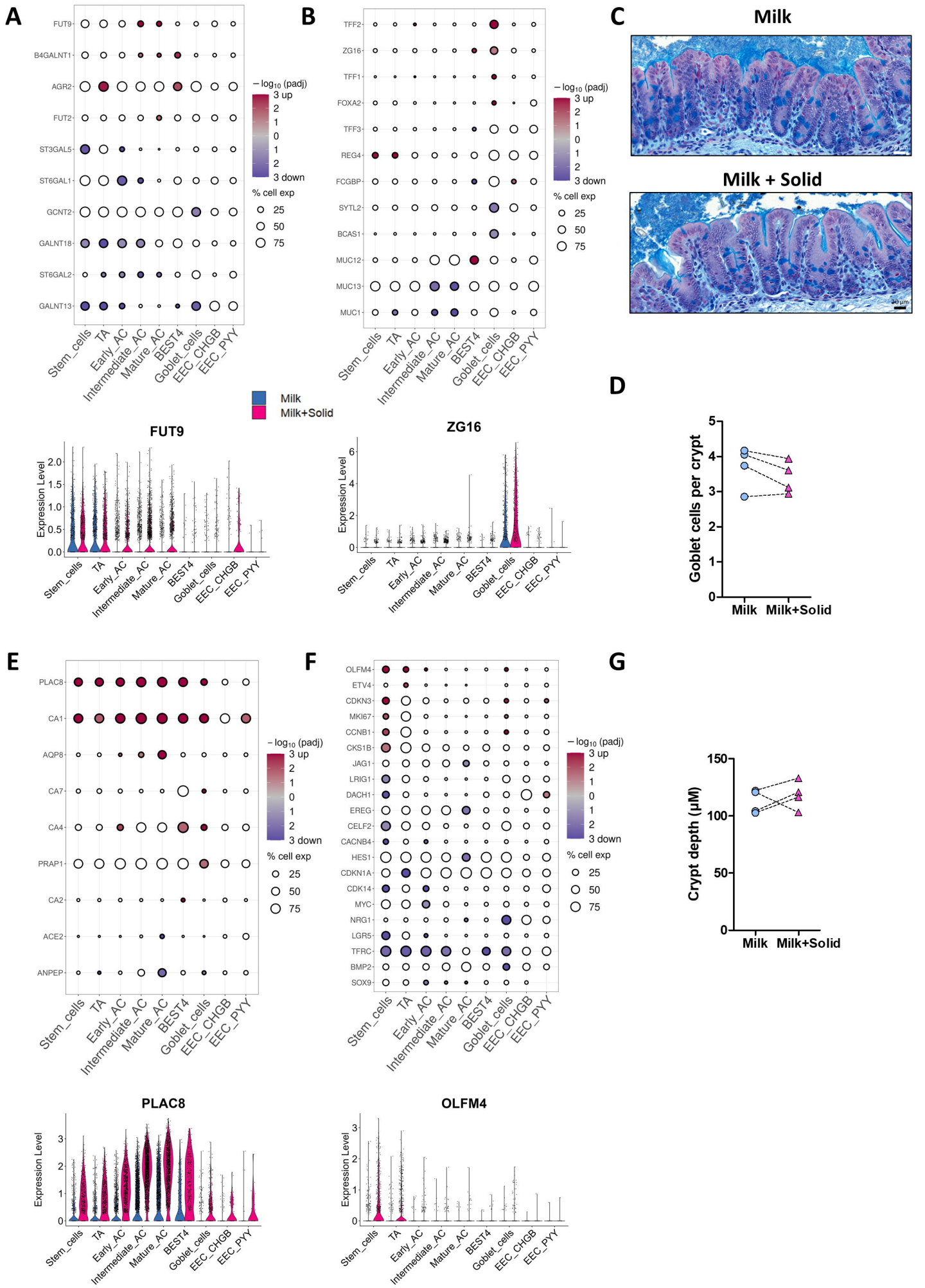
A
FUT9
B4GALNT1
AGR2
FUT2
ST3GAL5
ST6GAL1
GCNT2
GALNT18
ST6GAL2
GALNT13
Stem_cells
TA
Early_AC
Intermediate_AC
Mature_AC
BEST4
Goblet_cells
EEC_CHGB
EEC_PYY
− log10 (padj)
3 up
2
1
0
1
2
3 down
% cell exp
25
50
75
B
TFF2
ZG16
TFF1
FOXA2
TFF3
REG4
FCGBP
SYTL2
BCAS1
MUC12
MUC13
MUC1
C
Milk
Milk + Solid
Milk
Milk+Solid
FUT9
Expression Level
ZG16
D
Goblet cells per crypt
Milk
Milk+Solid
E
PLAC8
CA1
AQP8
CA7
CA4
PRAP1
CA2
ACE2
ANPEP
F
OLFM4
ETV4
CDKN3
MKI67
CCNB1
CKS1B
JAG1
LRIG1
DACH1
EREG
CELF2
CACNB4
HES1
CDKN1A
CDK14
MYC
NRG1
LGR5
TFRC
BMP2
SOX9
G
Crypt depth (μM)
Milk
Milk+Solid
PLAC8
OLFM4

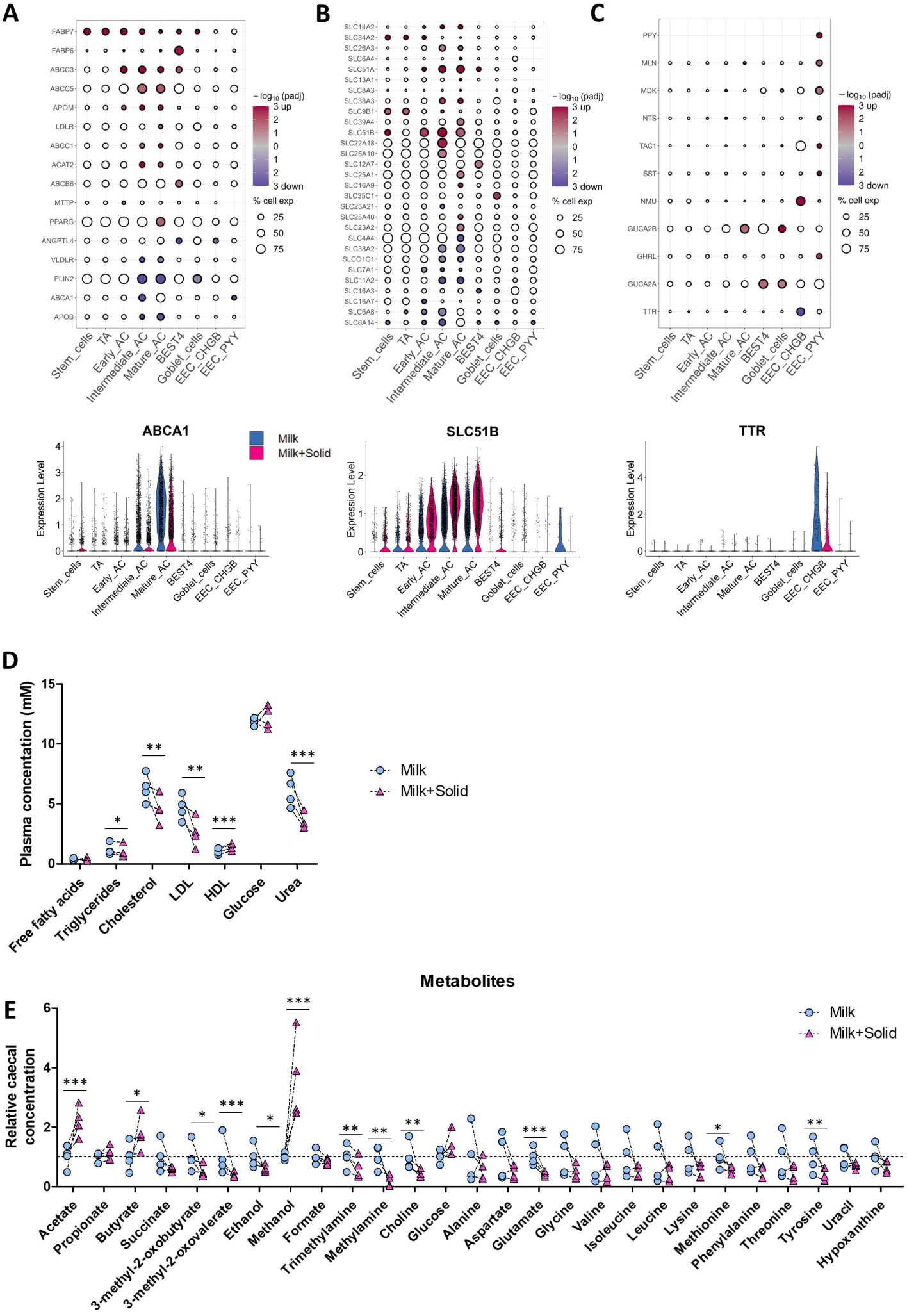
A
B
C
FABP7
FABP6
ABCC3
ABCC5
APOM
LDLR
ABCC1
ACAT2
ABCB6
MTTP
PPARG
ANGPTL4
VLDLR
PLIN2
ABCA1
APOB
SLC14A2
SLC34A2
SLC26A3
SLC6A4
SLC51A
SLC13A1
SLC8A3
SLC38A3
SLC9B1
SLC39A4
SLC51B
SLC22A18
SLC25A10
SLC12A7
SLC25A1
SLC16A9
SLC35C1
SLC25A21
SLC25A40
SLC23A2
SLC4A4
SLC38A2
SLCO1C1
SLC7A1
SLC11A2
SLC16A3
SLC16A7
SLC6A8
SLC6A14
PPY
MLN
MDK
NTS
TAC1
SST
NMU
GUCA2B
GHRL
GUCA2A
TTR
Stem_cells
TA
Early_AC
Intermediate_AC
Mature_AC
BEST4
Goblet_cells
EEC_CHGB
EEC_PYY
− log10 (padj)
3 up
2
1
0
1
2
3 down
% cell exp
25
50
75
ABCA1
SLC51B
TTR
Milk
Milk+Solid
Expression Level
D
Plasma concentation (mM)
Free fatty acids
Triglycerides
Cholesterol
LDL
HDL
Glucose
Urea
Milk
Milk+Solid
E
Metabolites
Relative caecal concentration
Acetate
Propionate
Butyrate
Succinate
3-methyl-2-oxobutyrate
3-methyl-2-oxovalerate
Ethanol
Methanol
Formate
Trimethylamine
Methylamine
Choline
Glucose
Alanine
Aspartate
Glutamate
Glycine
Valine
Isoleucine
Leucine
Lysine
Methionine
Phenylalanine
Threonine
Tyrosine
Uracil
Hypoxanthine
Milk
Milk+Solid